

Cycle flows and multistability in oscillatory networks

Cite as: Chaos 27, 083123 (2017); <https://doi.org/10.1063/1.4994177>

Submitted: 03 January 2017 • Accepted: 03 July 2017 • Published Online: 29 August 2017

Debsankha Manik, Marc Timme and  Dirk Witthaut



View Online



Export Citation



CrossMark

ARTICLES YOU MAY BE INTERESTED IN

[Multistability of phase-locking and topological winding numbers in locally coupled Kuramoto models on single-loop networks](#)

Journal of Mathematical Physics **57**, 032701 (2016); <https://doi.org/10.1063/1.4943296>

[A universal order parameter for synchrony in networks of limit cycle oscillators](#)

Chaos: An Interdisciplinary Journal of Nonlinear Science **27**, 073119 (2017); <https://doi.org/10.1063/1.4995963>

[Multistability in lossy power grids and oscillator networks](#)

Chaos: An Interdisciplinary Journal of Nonlinear Science **29**, 123119 (2019); <https://doi.org/10.1063/1.5122739>

APL Machine Learning

Open, quality research for the networking communities

Now Open for Submissions

LEARN MORE



Cycle flows and multistability in oscillatory networks

Debsankha Manik,¹ Marc Timme,^{1,2,3} and Dirk Witthaut^{4,5}

¹Network Dynamics, Max Planck Institute for Dynamics and Self-Organization (MPIDS), 37077 Göttingen, Germany

²Chair for Network Dynamics, Institute for Theoretical Physics and Center for Advancing Electronics Dresden (cfaed), Technical University of Dresden, 01069 Dresden, Germany

³Department of Physics, Technical University Darmstadt, 64289 Darmstadt, Germany

⁴Forschungszentrum Jülich, Institute for Energy and Climate Research - Systems Analysis and Technology Evaluation (IEK-STE), 52425 Jülich, Germany

⁵Institute for Theoretical Physics, University of Cologne, 50937 Köln, Germany

(Received 3 January 2017; accepted 3 July 2017; published online 29 August 2017)

We study multistability in phase locked states in networks of phase oscillators under both Kuramoto dynamics and swing equation dynamics—a popular model for studying coarse-scale dynamics of an electrical AC power grid. We first establish the existence of geometrically frustrated states in such systems—where although a steady state flow pattern exists, no fixed point exists in the dynamical variables of phases due to geometrical constraints. We then describe the stable fixed points of the system with phase differences along each edge not exceeding $\pi/2$ in terms of cycle flows—constant flows along each simple cycle—as opposed to phase angles or flows. The cycle flow formalism allows us to compute tight upper and lower bounds to the number of fixed points in ring networks. We show that long elementary cycles, strong edge weights, and spatially homogeneous distribution of natural frequencies (for the Kuramoto model) or power injections (for the oscillator model for power grids) cause such networks to have more fixed points. We generalize some of these bounds to arbitrary planar topologies and derive scaling relations in the limit of large capacity and large cycle lengths, which we show to be quite accurate by numerical computation. Finally, we present an algorithm to compute all phase locked states—both stable and unstable—for planar networks. © 2017 Author(s). All article content, except where otherwise noted, is licensed under a Creative Commons Attribution (CC BY) license (<http://creativecommons.org/licenses/by/4.0/>). [<http://dx.doi.org/10.1063/1.4994177>]

The functions of many networked systems in physics, biology, or engineering rely on a coordinated or synchronized dynamics of their constituents. In power grids for example, all generators must run at the same frequency and their phases need to lock to guarantee a steady power flow. Here, we analyze the existence and multitude of states exhibiting this phase locking behaviour. Focusing on edge and cycle flows instead of the nodal phases, we derive rigorous results on the existence and number of such states. Generally, multiple phase-locked states coexist in networks with edges capable of carrying high flows, long elementary cycles, and a homogeneous spatial distribution of natural frequencies or power injections. Utilizing concepts from the graph theory, we derive scaling relations for the number of such states in plane embedded networks. We also offer an algorithm to systematically compute all phase-locked states, both stable and unstable.

I. FROM KURAMOTO OSCILLATORS TO POWER GRIDS

Coupled oscillator models are ubiquitous in science and technology, describing the collective dynamics of various systems on micro- to macro-scale. Research on coupled oscillators dates back to Christian Huygens, who noticed that two clocks synchronize when they are coupled.¹ One of the

most important mathematical models was introduced by Kuramoto^{2,3} and successfully applied to describe the collective dynamics of coupled Josephson junctions,⁴ neuronal networks,⁵ chemical oscillators,⁶ and a variety of other synchronization phenomena.^{7–10}

That model³ describes the dynamics of N coupled limit cycle oscillators. The equations of motions for the phases θ_j , $j \in \{1, \dots, N\}$ are given by

$$\frac{d}{dt}\theta_j = \omega_j + \sum_{\ell=1}^N K_{j,\ell} \sin(\theta_\ell - \theta_j). \quad (1)$$

The coupling matrix is assumed to be symmetric, $K_{j,\ell} = K_{\ell,j}$, and ω_j are the natural frequencies of the oscillators. Throughout this article, we consider systems where all $K_{j,\ell} \geq 0$, i.e., the units attract each other and do not repel.

A similar model of second-order oscillators describes the collective phenomena of animal flocks^{11,12} or human crowds¹³ as well as the coarse-scale dynamics of power grids.^{14–20}

For power grids, for instance, the units j describe synchronous machines, generators, or motors, whose state is completely described by their phase θ_j and the phase velocity $\dot{\theta}_j$ relative to the reference frequency of the grid, typically rotating at 50 Hz or 60 Hz. The acceleration (deceleration) of the machines is proportional to the sum of the mechanical power P_j generated (consumed) by the machine including

damping and electric power exchanged with the grid. The detailed equations of motion are given by

$$M_j \frac{d^2}{dt^2} \theta_j + D_j \frac{d}{dt} \theta_j = P_j + \sum_{\ell=1} K_{j,\ell} \sin(\theta_\ell - \theta_j), \quad (2)$$

where M_j is an inertia term and D_j a damping constant. The coupling constants $K_{j,\ell} = U^2 B_{j,\ell}$ are determined by the voltage U of the grid, which is assumed to be constant, and the admittance $B_{j,\ell}$ of the electrical transmission line joining node j and node ℓ . The flow of electric real power from node ℓ to node j is

$$F_{j,\ell} = K_{j,\ell} \sin(\theta_\ell - \theta_j) = K_{j,\ell} S_{j,\ell}. \quad (3)$$

It is useful to describe the interaction topology of the system as a weighted graph $G(V, E)$, whose vertex set V is identical to the set of oscillators and edge set E is given by the set of all inter-oscillator coupling pairs, i.e., all pairs with $K_{\ell,j} > 0$. We use the term network²¹ (rather than the term graph) for the entire system with given natural frequencies ω_j or the powers P_j .

Here, we distinguish two types of synchronization in oscillator networks. Traditionally, the emergence of partial synchrony has received the most interest of the physics community.^{2,3,7,8} In his seminal work, Kuramoto investigated a set of oscillators with global coupling, $K_{j,\ell} = K/N$, and natural frequencies drawn at random from a unimodal symmetric distribution $g(\omega)$. If the coupling constant K exceeds a critical value K_c , a fraction of the oscillators start to synchronize in the sense that they rotate at the same angular velocity although their natural frequencies differ. In this state of *partial frequency locking*, commonly referred to in the Kuramoto oscillator literature as “partial synchrony,”⁸ the phases of parts of the oscillators are ordered, but they are not strictly phase-locked, such that the phase difference of two synchronized oscillators ($\theta_j - \theta_\ell$) is generally small but not constant.

In this article, we analyze the properties of *globally phase-locked states*, where all oscillators synchronize and the phase differences ($\theta_j - \theta_\ell$) are constant for all pairs (j, ℓ) . These states are especially important for power grids, as they describe the regular synchronous operation of the grid.^{14–18} If this state is lost due to local outages or accidents, the grid will fragment into asynchronous islands which can no longer exchange electric energy.²² For instance, the European power grid fragmented into three asynchronous areas on November 4th 2006 after the shutdown of one transmission line in Northern Germany. As a result, southwestern Europe suffered an under-supply on the order of 10 GW and approximately 10 million households were disconnected.²³

Without loss of generality, we take $\sum_j \omega_j = 0$ or $\sum_j P_j = 0$, respectively, by invoking a transformation to a co-rotating frame of reference. The globally phase-locked states are then the *fixed points* of the system. For both the Kuramoto model and the power grid model, these states are given by the solutions of the transcendental equations

$$P_j + \sum_{\ell=1}^N K_{j,\ell} \sin(\theta_\ell - \theta_j) = 0 \quad \text{for all } j \in \{1, \dots, N\}, \quad (4)$$

replacing P_j by ω_j for the Kuramoto model. In the following, we analyze the influence of the network topology given by the coupling matrix $K_{j,\ell}$ on the existence of a fixed point. All results below hold for both models; nevertheless, our intuition heavily relies on the interpretation of $F_{j,\ell} = K_{j,\ell} \sin(\theta_\ell - \theta_j)$ as a flow which is inspired from the power grid model. The results can be generalized to arbitrary coupling functions f instead of the sine (see, e.g., Refs. 24 and 25). In the following, we mostly restrict ourselves to the common sine coupling for the sake of clarity.

We note that the second order power grid model (2) evidently describes a different system from the first order Kuramoto model (1). Nevertheless, there are deep underlying connections between these two. In the context of power grids, in the overdamped limit, one recovers the first order Kuramoto model. The relation of first and second order models in the context of coupled Josephson Junctions was discussed in detail in Refs. 26 and 27. Partial synchronization in first and second order models was reviewed in Ref. 28.

II. THE NATURE AND BIFURCATIONS OF FIXED POINTS

Both the Kuramoto system and the oscillator model of power grids share the same set of fixed points (4). It has been shown that the similarity between these two systems runs deeper, namely, the linear stability properties of those fixed points are identical.^{29,30} In this section, we briefly review some basic results on the stability of the fixed points.

We analyze the dynamical stability of a certain fixed point $\theta^* = (\theta_1^*, \dots, \theta_N^*)$ by defining the potential function

$$V(\theta_1, \theta_2, \dots, \theta_N) = - \sum_j P_j \theta_j - \frac{1}{2} \sum_{ij} K_{ij} \cos(\theta_i - \theta_j). \quad (5)$$

The fixed points correspond to the local extrema of this potential, where $\frac{\partial V}{\partial \theta_j} = 0$ for all j . A fixed point θ^* is asymptotically stable if the Hesse matrix H of the potential function

$$H(\theta^*) = \begin{pmatrix} \sum_{\ell} K_{1,\ell}^{\text{red}} & -K_{1,2}^{\text{red}} & \dots \\ -K_{2,1}^{\text{red}} & \sum_l K_{2,\ell}^{\text{red}} & \dots \\ \vdots & \vdots & \ddots \end{pmatrix} \quad (6)$$

with the residual capacity

$$K_{j,\ell}^{\text{red}} = K_{j,\ell} \cos(\theta_j^* - \theta_\ell^*) \quad (7)$$

has positive eigenvalues only. It is worth noting that H has one eigenvector $v_1 = (1, 1, \dots, 1)$ with eigenvalue $\mu_1 = 0$ because any fixed point θ^* is arbitrary up to an additive constant c . As such a global phase shift does not affect the locking of the phases, we can discard it in the following and concentrate on the stability transversely to the solution space $\{\theta^* + c(1, 1, \dots, 1) | c \in \mathbb{R}\}$.

Lemma 1. Let the eigenvalues of H be ordered such that $\mu_1 = 0$ and $\mu_2 \leq \dots \leq \mu_N$. If for a given network topology and a given fixed point,

$$\mu_k > 0, \quad \text{for all } k \in \{2, 3, \dots, N\}, \quad (8)$$

then this fixed point is transversally asymptotically stable for both the Kuramoto system and the power grid model system. If one of the $\mu_k < 0$, then the dynamical system is linearly unstable (this lemma and its proof have been presented in Ref. 29).

Using some results from the bifurcation theory, it has been shown in Ref. 29 that a stable fixed point can only be lost by an inverse saddle-node bifurcation when one of the eigenvalues becomes zero, $\mu_2 = 0$. At this point, linear stability analysis is not sufficient to predict the stability of the fixed point, but it is expected that the fixed point is unstable.³¹

More insights into the loss of a fixed point when the phase differences across all edges in the network are sufficiently small can be gained:

Corollary 1. Consider a connected network. It is sufficient (but not necessary) for a fixed point θ^* to be transversally asymptotically stable; if the condition

$$\cos(\theta_i^* - \theta_j^*) > 0 \quad (9)$$

holds for all edges (i, j) in the network, then the network is said to be in “normal operation.”

Proof. To this end, we first define a metagraph as follows.

Definition 1 (Metagraph). Given a graph $G(V, E)$ and a set of flows F_{uv} across each edge $e(u, v)$, its metagraph \tilde{G} is an undirected graph with vertex set V and edge set E' defined as follows. For all edges $e(u, v) \in E$, with weight K_{uv} , \exists , an edge $e(u, v) \in E'$ with weight $K_{uv}^{\text{red}} = \sqrt{K_{uv}^2 - F_{uv}^2}$, as per (7).

Then, the matrix H as defined in (6) is seen to be the Laplacian matrix of the metagraph \tilde{G} . The eigenvalues of a Laplacian of a connected undirected graph with positive edge weights are always non-negative²¹ such that we obtain the result. \square

We note that this sufficient condition for stability has been shown in Ref. 32 using the Gershgorin circle theorem.

During normal operation, an eigenvalue of the Hesse matrix H , as defined in (6), can become 0 only when \tilde{G} disconnects into two (or more) components. Such a split-up occurs only when $K_{j,\ell}^{\text{red}} = 0$ for all the transmission lines connecting two certain parts (denoted by G_1 and G_2) of the network, meaning that these lines are completely saturated

$$\begin{aligned} \sin(\theta_j^* - \theta_\ell^*) = \pm 1 &\Rightarrow |F_{j,\ell}| = K_{j,\ell} \\ \text{for all } (j, \ell) \in E, j \in G_1, \ell \in G_2. &\quad (10) \end{aligned}$$

Another scenario for the loss of stability is that one or more transmission lines leave normal operation. Then, the edge weights become effectively negative, such that a simple graph-theoretic interpretation of the bifurcation is no longer possible.^{29,58}

III. CYCLE FLOWS AND GEOMETRIC FRUSTRATION

A. Flow conservation and the dynamics condition

It is instructive to divide the defining equation (4) of a fixed point into two parts. First, every fixed point has to satisfy a dynamic condition which is nothing but the conservation of the flow at every node of the network

$$P_j + \sum_{\ell=1}^N K_{j,\ell} S_{j,\ell} = 0 \quad \text{for all } j \in \{1, \dots, N\}, \quad (11a)$$

$$|S_{j,\ell}| \leq 1 \quad \text{for all edges } (j, \ell). \quad (11b)$$

Here, $\sum_{\ell} K_{j,\ell} S_{j,\ell}$ is the sum of all flows from the neighboring nodes to the node j , while P_j is a source or sink term. The second part of this condition reflects the fact that the transmission capacity of each link is bound, such that the magnitude of the flow $|F_{j,\ell}|$ cannot exceed the capacity $K_{j,\ell}$. The dynamic condition (11) holds for all flow networks also including DC networks (i.e., Kirchhoff’s rules) and biological network models.^{33,34}

To obtain a better understanding of the possible solutions, we slightly rephrase the dynamic condition (11). In particular, we label all the L edges in the network with $e \in \{1, \dots, L\}$. As the flows are directed, we have to keep track of the ordering of the vertices connected by the edge e . That is, each e corresponds to a directed link (j, ℓ) in the following. The ordering is arbitrary but must be kept fixed. Then, we write $S_e = S_{j,\ell}$ and $F_e = F_{j,\ell}$ for the flow over a link $e \hat{=} (j, \ell)$. Furthermore, we define the unweighted edge incidence matrix $I \in \mathbb{R}^{N \times L}$ (Ref. 21) via

$$I_{j,e} = \begin{cases} +1 & \text{if node } j \text{ is the head of edge } e \hat{=} (j, \ell), \\ -1 & \text{if node } j \text{ is the tail of edge } e \hat{=} (j, \ell), \\ 0 & \text{otherwise,} \end{cases} \quad (12)$$

and the weighted edge incidence matrix $\tilde{K} \in \mathbb{R}^{N \times L}$ with the components $\tilde{K}_{j,e} = K_e I_{j,e}$.

The dynamic condition (11) then reads

$$P_j + \sum_{e=1}^L I_{j,e} F_e = 0 \quad \text{for all } j = 1, \dots, N, \quad (13a)$$

$$|F_e| \leq K_e \quad \text{for all } e = 1, \dots, L \quad (13b)$$

in terms of the flows or

$$P_j + \sum_{e=1}^L \tilde{K}_{j,e} S_e = 0 \quad \text{for all } j = 1, \dots, N, \quad (14a)$$

$$|S_e| \leq 1 \quad \text{for all } e = 1, \dots, L \quad (14b)$$

in terms of the sine factors. Here, $\mathbf{F} = (F_1, \dots, F_L)^T$ and $\mathbf{S} = (S_1, \dots, S_L)^T$ are vectors in \mathbb{R}^L . The matrix \tilde{K} has N rows, but its rank is only $(N - 1)$. This is due to the fact that the sum of all rows is zero as $\sum_j \tilde{K}_{j,e} = 0$ since each edge has exactly one head and one tail. Hence, the solutions of the linear set of Eq. (14a) span an affine subspace of \mathbb{R}^L whose dimension is $(L - N + 1)$. This statement will later be

rigorously proved in Lemma 2. In many important applications, L is much larger than the number of nodes N , such that we have a high dimensional submanifold \mathbb{B} of \mathbb{R}^L with every $S \in \mathbb{B}$ being a solution of (14) and hence a candidate for a fixed point of (1) and (2). However, the set of solutions of the dynamical equations can also be empty if the capacities $K_{j,\ell}$ are too small. In fact, the condition (14b) defines a bound convex polytope in \mathbb{R}^L . The solution of the full dynamical conditions (14) is given by the intersection of this polytope and the $(L - N + 1)$ dimensional affine subspace.

We can further characterize the solution of the dynamic conditions by establishing that the homogeneous solutions of the system (14a) are just the *cycle flows* which do not affect flow conservation. As the number of fundamental cycles in a network is $(L - N + 1)$, the dimension of the solution space is also given by $(L - N + 1)$. The derivation of these results is as follows.

Definition 2 (Simple cycle). Given an undirected graph $G(V, E)$, a closed path $c = (v_1, v_2, \dots, v_l, v_1)$ where no vertex apart from v_1 occurs twice is called a simple cycle (Ref. 36, p. 21).

Definition 3 (Cycle basis). Given a connected graph $G(V, E)$ with L edges and N vertices, the set of all simple cycles \mathfrak{C} forms a vector space over the two element field $GF(2) = \{0, 1\}$, with the set symmetric difference being the addition operator. This vector space has dimension $L - N + 1$. A basis B_C of this vector space is called a *cycle basis* of the graph G .

Definition 4 (Signed characteristic vector of a cycle). An arbitrary assignment of a direction to each edge of an undirected graph G , which results in a directed graph, is called an orientation G^σ .³⁶ Given a graph G with L edges and N vertices and one such orientation, there exists an injective mapping from the set \mathfrak{C} of all simple cycles of G to \mathbb{R}^L as follows:

$$\begin{aligned} \mathfrak{C} &\rightarrow \mathbb{R}^L, \\ c &\mapsto z^c, \\ z_e^c &= \begin{cases} 0, & \text{if } e \text{ is not in } c, \\ 1, & \text{if } e = (v_i, v_{i+1}) \text{ and } v_{i+1} \text{ is the head of } e, \\ -1, & \text{if } e = (v_i, v_{i+1}) \text{ and } v_{i+1} \text{ is the tail of } e. \end{cases} \end{aligned}$$

z^c is called the *signed characteristic vector* of each cycle.

Now, we show that any fixed point of the system can be uniquely specified by a *cycle flow* along each cycle belonging to a cycle basis of the underlying graph, along with an arbitrary solution of (13).

Definition 5 (Cycle flow). Given a simple cycle $c = (v_1, v_2, \dots, v_l, v_1)$ belonging to an undirected graph $G(V, E)$, a flow \mathbf{F} is called a *cycle flow* if

$$F_{j,k} = \begin{cases} f_c & \text{if } (j,k) \in \{(v_1, v_2), (v_2, v_3), \dots, (v_{l-1}, v_l), (v_l, v_1)\}, \\ 0 & \text{otherwise,} \end{cases} \tag{15}$$

i.e., it is a constant nonzero flow along the cycle.

Lemma 2. Let \mathbb{S}_G be the set of all fixed points of a network G satisfying the normal operation criteria (9). Then,

there exists a one-to-one function $f_c : \mathbb{S}_G \mapsto \mathbb{R}^{L-N+1}$ that maps each fixed point to a cycle flow vector.

Proof. Let $\theta^{(0)}$ be one (arbitrarily chosen) fixed point. Let θ be another. Then, we construct the mapping f_c by proving that the flows for these two fixed point differ only by *cycle flows* along each cycle.

Let $\mathbf{F}^{(0)} = (F_{e_1}^{(0)}, F_{e_2}^{(0)}, \dots, F_{e_L}^{(0)})$ and $\mathbf{F} = (F_{e_1}, F_{e_2}, \dots, F_{e_L})$ be the flows for the fixed points $\theta^{(0)}$ and θ , respectively. Then,

$$\mathbf{F} - \mathbf{F}^{(0)} = \sum_{c \in B_C} f_c z^c, \tag{16}$$

due to the result from the graph theory that the flow space of an oriented graph G^σ is spanned by the signed characteristic vectors (Definition 4) of its cycles (Ref. 37, p. 311). Since by definition the cycles in B_C form a basis of the cycle space, the coefficients f_c are guaranteed to be unique. This concludes the proof. \square

We note that this mapping between fixed points and cycle flows has previously been presented in slightly different ways in Refs. 18 (supplementary material) and 38.

B. The winding number and the geometric condition

In addition to the dynamic condition, there is a geometric condition for the existence of a fixed point: a fixed point exists if the flows $F_{j,\ell} = K_{j,\ell} S_{j,\ell}$ satisfy the dynamic condition (14) and if

$$\text{for all edges } (\ell, j) : \exists (\theta_1, \dots, \theta_N) \text{ such that } S_{j,\ell} = \sin(\theta_\ell - \theta_j). \tag{17}$$

We now rephrase this condition in a more instructive way. To this end, we assume that we have already obtained a solution of the dynamic condition (14). Then, we can try to successively assign a phase θ_j to every node j in the network. Starting at a node j_0 with an arbitrary phase θ_{j_0} , we assign the phases of all neighboring nodes j_1 such that $\sin(\theta_{j_1} - \theta_{j_0}) = S_{j_0, j_1}$. We then proceed in this way through the complete network to assign the phase of an arbitrary node j_n ,

$$\theta_{j_n} = \theta_{j_0} + \sum_{s=0}^{n-1} \Delta_{j_s, j_{s+1}}, \tag{18}$$

where (j_0, j_1, \dots, j_n) is an arbitrary *path* from j_0 to j_n and we have used a solution of the equation

$$S_{j,\ell} = \sin(\Delta_{j,\ell}) \tag{19}$$

for every edge (j, ℓ) .

In general, a given node j_n can be reached from j_0 via a multitude of different paths. To define a unique set of phases that satisfy the geometric condition (17), we must ensure that Eq. (18) yields a unique phase regardless of which path is taken from j_0 to j_n . This is equivalent to the condition that the phase differences over every *simple cycle* (as defined in Definition 2) in the network must add up to an integer multiple of 2π .

$$\sum_{(j,\ell) \in \text{cycle } c} \Delta_{j,\ell} = 2m\pi, \quad \text{for some } m \in \mathbb{Z}, \quad (20)$$

where $\Delta_{j,\ell}$ is a solution of Eq. (19). Furthermore, it is sufficient if (20) is satisfied by the cycles in the cycle basis of the network defined in Definition 3: it will then automatically be satisfied for all simple cycles of the network since the simple cycles form a vector space.

However, there are two distinct solutions

$$\Delta_{j,\ell}^+ = \arcsin(S_{j,\ell}), \quad (21a)$$

$$\Delta_{j,\ell}^- = \pi - \arcsin(S_{j,\ell}) \quad (21b)$$

of Eq. (19) which satisfy $\Delta_{j,\ell}^\pm \in [-\pi, \pi)$. To consider both, we define a partition of the edge set

$$E = E_+ \cup E_-, \quad (22)$$

$$E_+ = \{(j, \ell) \in E \mid \Delta_{j,\ell} = \Delta_{j,\ell}^+\}, \quad (23)$$

$$E_- = \{(j, \ell) \in E \mid \Delta_{j,\ell} = \Delta_{j,\ell}^-\}. \quad (24)$$

Alternatively, we can define the two sets in terms of the nodal phases as

$$E_+ = \{(i, j) \in E \mid \cos(\theta_i - \theta_j) > 0\}, \quad (25)$$

$$E_- = \{(i, j) \in E \mid \cos(\theta_i - \theta_j) \leq 0\}. \quad (26)$$

We note that a fixed point where the plus sign is realized for all edges ($E_- = \{\}$) is guaranteed to be linearly stable according to corollary 1. We refer to it as *normal operation*.

To operationalize the geometric condition, we now define the winding number (27) following the terminology used by Ochab and Gora³⁸ and Wiley *et al.*³⁹

Definition 6 (*Winding vector*). Consider a connected network with flows \mathbf{F} . For every fundamental cycle c , the winding number with respect to a partition $E = E_+ + E_-$ is defined as

$$\varpi_c = \frac{1}{2\pi} \sum_{e \in E} z_e^c \Delta_e(F_e) \quad (27)$$

with

$$\Delta_e(F_e) = \begin{cases} \arcsin(F_e/K_e) & \text{for } e \in E_+ \\ \pi - \arcsin(F_e/K_e) & \text{for } e \in E_- \end{cases} \quad (28)$$

The winding vector is defined as

$$\boldsymbol{\varpi} = (\varpi_1, \dots, \varpi_{L-N+1})^T. \quad (29)$$

Using the winding number, we can reformulate the conditions for the existence of a fixed point and establish a correspondence between the description of fixed points in terms of nodal phases of edge flows.

Theorem 7. Consider a connected network with power injections $\mathbf{P} \in \mathbb{R}^N$ and coupling matrix $\mathbf{K} \in \mathbb{R}^{N \times N}$. Then, the following two statements are equivalent:

1. $\boldsymbol{\theta}^*$ is a fixed point, i.e., a real solution of Eq. (4).

2. $\mathbf{F} \in \mathbb{R}^L$ satisfies the dynamic condition (13) and $\boldsymbol{\varpi} \in \mathbb{Z}^{L-N+1}$ for some partition $E = E_+ + E_-$.

Proof. We prove the theorem in two parts.

(1) \Rightarrow (2): If $\boldsymbol{\theta}^*$ is a fixed point, then the flows \mathbf{F} satisfying the dynamical condition (13) as given by (3) are

$$F_{j,k} = K_{j,k} \sin(\theta_k - \theta_j). \quad (30)$$

Let us partition the edge set into E^+ and E^- by

$$e = (j, k) \in \begin{cases} E^+ & \text{if } \cos(\theta_k - \theta_j) > 0 \\ E^- & \text{if } \cos(\theta_k - \theta_j) \leq 0. \end{cases} \quad (31)$$

We note the identity that

$$\begin{aligned} \arcsin(\sin(x)) &= \begin{cases} -x + (2m_x + 1)\pi & \text{if } \cos(x) \leq 0 \\ x + 2m_x\pi & \text{if } \cos(x) > 0, \text{ for some } m_x \in \mathbb{Z}. \end{cases} \end{aligned} \quad (32)$$

Combining this identity with the definition of Δ_e in (28) and our chosen set partition (31) results in

$$\begin{aligned} \text{for all } (j, k) \in E^+, \quad \Delta_{j,k} &= \arcsin(F_{jk}/K_{jk}), \\ &= \arcsin(\sin(\theta_k - \theta_j)), \\ &= 2m_{jk}\pi + (\theta_k - \theta_j), \end{aligned} \quad (33)$$

$$\begin{aligned} \text{for all } (j, k) \in E^-, \quad \Delta_{j,k} &= \pi - \arcsin(F_{jk}/K_{jk}), \\ &= \pi - \arcsin(\sin(\theta_k - \theta_j)), \\ &= -2m_{jk}\pi + (\theta_k - \theta_j). \end{aligned} \quad (34)$$

Combining (33) and (34), we obtain $\Delta_{jk} = 2m_{jk}\pi + (\theta_k - \theta_j)$, $m_{jk} \in \mathbb{Z}$ (choosing the + sign for $2m_{jk}\pi$ without loss of generality).

Then, for any simple cycle $c = (v_1, v_2, \dots, v_l, v_1)$ in the cycle basis B_C , the winding number is

$$\varpi_c = \frac{1}{2\pi} \sum_{e \in E} z_e^c \Delta_e(F_e), \quad (35)$$

$$= (m_{12} + m_{23}, \dots, m_{l1}) \in \mathbb{Z}, \quad (36)$$

thus completing the first part of the proof.

(2) \Rightarrow (1): Given a set of flows satisfying the dynamic condition (13) and having integral winding numbers, the fixed point $\boldsymbol{\theta}^*$ can be constructed following Eqs. (17) and (18).

This concludes the proof. \square

C. Geometric frustration

The previous reasoning shows that we can face the following situation: given an oscillator network characterized by the frequencies P_j and the capacity matrix $K_{j,\ell}$, we can find a solution of the dynamical conditions, such that the flow is conserved at all nodes of the network. Nevertheless, no fixed point exists as these solutions are incompatible with the geometric conditions. In this case, we say that phase locking is inhibited due to *geometric frustration*. We

summarize this in a formal definition before giving some examples for the importance of this phenomenon.

Definition 8. An oscillator network is said to be geometrically frustrated if a solution of the dynamic conditions (11) exists, but all solutions are incompatible with the geometric conditions (20) such that no fixed point exists.

This definition builds on a generalized notion of geometric frustration introduced in mathematical physics.⁴⁰ In that context, a system with multiple state variables (x_1, x_2, \dots, x_n) is called geometrically frustrated if for certain pair-wise correlations between those variables, no steady state exist satisfying all these correlations simultaneously.

IV. EXAMPLES AND APPLICATIONS

In this section, we discuss the importance of geometric aspects for the fixed points of an oscillator network with different topologies. In particular, we analyze the number of fixed points and show that geometric frustration can inhibit phase locking, which may lead to counter-intuitive phenomena.

A. Trees do not suffer from frustration

By definition, a tree does not contain any cycle such that the geometric condition (20) does not apply. Therefore, the calculation of a fixed point of the power grid oscillator model and the Kuramoto model as defined by Eq. (4) on a tree reduces to the solution of the dynamic condition (11), which is a linear set of equations. Moreover, we can find a strong result on the number of stable and unstable fixed points—see Corollary 2.

B. Multiple solutions in the cycle

We now consider the simplest nontrivial topology of a cyclic network with only three nodes and three links with equal strength K . The dynamical condition for the existence of a fixed point then reads

$$K \begin{pmatrix} 0 & 1 & -1 \\ -1 & 0 & 1 \\ 1 & -1 & 0 \end{pmatrix} \begin{pmatrix} S_{1,2} \\ S_{2,3} \\ S_{3,1} \end{pmatrix} = \begin{pmatrix} P_3 \\ P_1 \\ P_2 \end{pmatrix} \quad (37)$$

and $|S_{j,\ell}| \leq 1$. In particular, for $P_j = 0$, any solution is a cycle flow $(S_{1,2}, S_{2,3}, S_{3,1}) = S \times (1, 1, 1)$.

Taking into account that there are two possible solutions for the phase difference along each edge as per (21) and since in order to satisfy the geometric condition (20), the sum of phase differences along the cycle must equal $2m\pi$ for some integer $m \in \mathbb{Z}$, we see that all fixed points must satisfy

$$\Delta_{12}^\pm + \Delta_{23}^\pm + \Delta_{31}^\pm = 2m\pi. \quad (38)$$

Taking all combinations of either Δ^+ or Δ^- and corresponding possible values of m , we see that there are three intersections corresponding to three fixed points. These fixed points are illustrated in Fig. 1. This shows that stationary states are generally not unique, not even for the simplest cycle network. In the present case, only one of the solutions is dynamically stable, but this is generally not true in larger cycles as we will show in the following.

C. Frustration induces discreteness

We now extend the above example to a single cycle with an arbitrary number of nodes with the same power $P_j \equiv 0$. All links have an equal strength K as above. For the sake of notational convenience, we label the nodes as $1, 2, \dots, N$ along the cycle and identify node 1 with $N + 1$ and 0 with N . In order to have a non-trivial closed cycle, we need $N \geq 3$. The dynamic conditions for fixed points are then given by

$$F_{j+1,j} = F_{j,j-1} \equiv F \quad \text{for all } j = 1, \dots, N, \quad (39)$$

$$|F| \leq K. \quad (40)$$

We stress that the dynamic conditions have a continuum of solutions, i.e., all F values in the interval $[-K, K]$ are allowed.

The phase difference along the edges $(j + 1, j)$ is given by Eq. (21), leaving two possible solutions $\Delta_{j,\ell}^+$ and $\Delta_{j,\ell}^-$. Choosing the minus sign for at least one edge $(\ell + 1, \ell)$ yields $\tilde{K}_{\ell+1,\ell}^{\text{red}} = -\sqrt{K^2 - F^2} < 0$. In this case, one can show that the Hesse matrix H is not positive semi-definite such that the fixed point must be unstable. Restricting ourselves to the dynamically stable states, we find that the phase differences are all equal and given by

$$\theta_{j+1} - \theta_j = \arcsin(F/K). \quad (41)$$

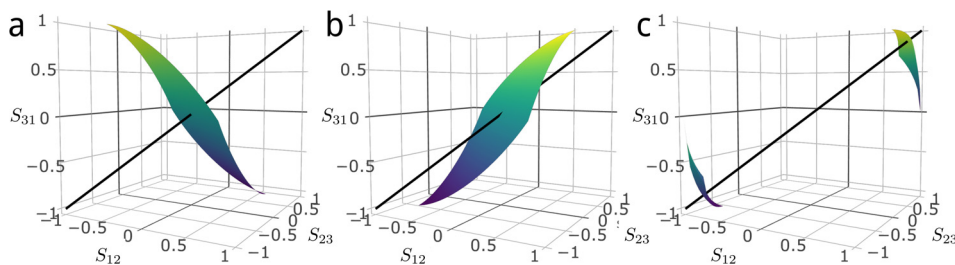


FIG. 1. Illustration of geometric frustration and multistability in the simplest cyclic network with 3 nodes with $P_j = 0$ and three links with equal strength K . Subplots show different branches of (38) obtained by choosing + or - sign for Δ_{12}, Δ_{23} , and Δ_{31} . The black lines denote the solution space of the dynamical condition (37), $S_{1,2} = S_{2,3} = S_{3,1} = S$. (a) Branch $(+++)$ with $m = 0$. (b) Branch $(--+)$ with $m = 1$. The branches $(+-)$ and $(-+)$ yield solutions at $S = (0, 0, 0)$ in an analogous way. (c) Branch $(---)$ with $m = 1$ (upper part) and $m = 2$ (lower part). The branches $(+ +-)$, $(+ - +)$, and $(- + +)$ do not yield a solution.

The geometric condition now yields

$$N \arcsin(F/K) = 0 \pmod{2\pi}, \quad (42)$$

which can be satisfied only for certain *discrete* values of F . The geometric condition thus induces a “quantization” of the phase differences as previously reported in Refs. 37 and 39

$$\theta_{j+1} - \theta_j = \frac{n}{N} 2\pi, \quad (43)$$

$$\text{with } n \in \left\{ -\left\lfloor \frac{N-1}{4} \right\rfloor, -\left\lfloor \frac{N-1}{4} \right\rfloor + 1, \dots, +\left\lfloor \frac{N-1}{4} \right\rfloor \right\},$$

where $\lfloor \cdot \rfloor$ denotes the floor function. We note that solutions with $(\theta_{j+1} - \theta_j) = \pm\pi/2$ have Jacobian eigenvalues $\mu_k = 0$ for all $k \in \{1, \dots, N\}$. In this case, linear stability analysis fails to determine dynamical stability properties (see the study by Khazin und Shnol³¹ for details). For two coupled oscillators, it is rather easy to see that the fixed point is nonlinearly unstable. In total, we thus find $2 \times \lfloor (N-1)/4 \rfloor + 1$ different stable stationary states.

This example is very simple but illustrates three important general results. First, there can be *multiple* stable fixed points in cyclic networks as previously noticed in Refs. 38 and 41–43. This fact has been discussed in power engineering in Ref. 44, but rigorous results on conditions on the existence of multistability and the number of fixed points are rare probably because most authors in this community concentrate on fully connected networks which arise after a Kron reduction.^{17,41} Second, the oscillator model (2) allows for stable fixed points with a persistent current around a cycle. Interestingly, these states are phase locked but *not phase ordered* in the sense that the phase order parameter⁷

$$r e^{i\psi} := \frac{1}{N} \sum_j e^{i\theta_j} \quad (44)$$

vanishes exactly for $K > 0$. Third, the geometric condition induces the *discreteness* of the phase differences although the dynamic condition allows for continuous values of cycle flows.

D. Braess' paradox

Here, we introduce a special example which illustrates the paradoxical effects of geometric frustration most clearly. We consider the oscillator network depicted in Fig. 2(a) consisting of $N=4$ nodes placed on a cyclic network, where nodes 1 and 3 have power injection $-P$ and nodes 2 and 4 have power injections P . In particular, we analyze what happens if the capacity of the upper edge (1, 2) is increased from K to $K' = K + \kappa$.

The dynamic condition for this network reads

$$0 = P_j + (K_{j+1,j} S_{j+1,j} - K_{j,j-1} S_{j,j-1}), \quad (45)$$

and $|S_{j+1,j}| \leq 1$, identifying node $j=5$ with $j=1$. For notational convenience, we define the vector

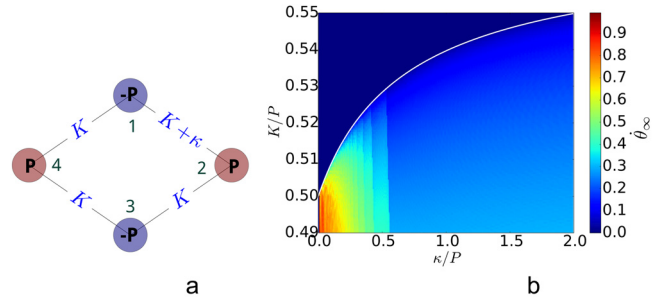


FIG. 2. Geometric frustration induces Braess' paradox. (a) Topology of the network under consideration. (b) Average phase velocities $\hat{\theta}_\infty$ defined in (49) for different values of K and κ . For fixed points, $\hat{\theta}_\infty = 0$. The white line shows the critical coupling K_c . The fixed point can be lost when the local transmission capacity κ increases.

$$\mathbf{S} = (S_{4,1}, S_{1,2}, S_{2,3}, S_{3,4}). \quad (46)$$

The solutions of the linear system of Eq. (45) span a one-dimensional affine space parametrized by a real number ϵ ,

$$\mathbf{S} = \frac{P}{K} (\mathbf{S}_a - \epsilon \mathbf{S}_b). \quad (47)$$

The vector $\mathbf{S}_a = (-1, 0, -K/K', 0)$ is an inhomogeneous solution of the linear system (45), and the vector $\mathbf{S}_b = (1, 1, K/K', 1)$ is a homogeneous solution corresponding to a cycle flow. Evaluating the condition $|S_{j+1,j}| \leq 1$ yields a necessary condition for the existence of a fixed point

$$2K \geq P. \quad (48)$$

For $\kappa=0$, this condition is also sufficient for the existence of a stable fixed point. If the capacity of the upper link increases, $\kappa > 0$, geometric frustration inhibits phase locking. A solution of the dynamical conditions always exists for $2K \geq P$, but this can become incompatible with the geometric condition. We illustrate this in the stability diagram in Fig. 2(b). A stable fixed point exists only in the parameter region above the white line. As we see in Fig. 2(b), the minimum K required to maintain steady operation, the *critical coupling* K_c , increases when κ is increased.

To further characterize the long-time behavior of the oscillator network, we define $\hat{\theta}_\infty$ as the average phase velocities of all the nodes in the limit of large time

$$\hat{\theta}_\infty = \lim_{T \rightarrow \infty} \frac{1}{\tau} \int_T^{T+\tau} \frac{1}{N} \sum_{j=1}^N |\dot{\theta}_j(t)| dt. \quad (49)$$

Therefore, $\hat{\theta}_\infty$ must be zero for steady operation to take place. As expected, we find $\hat{\theta}_\infty = 0$ in the stable parameter region above the white line $K > K_c$ and $\hat{\theta}_\infty > 0$ in the unstable parameter region below the white line $K < K_c$. Remarkably, $\hat{\theta}_\infty$ is the largest for small values of κ and, of course, $K < K_c(\kappa)$.

This leads to the paradoxical effect that an increase in local transmission capacity reduces the ability of the network to support a phase locked fixed point. This behavior can also be seen as an example of Braess' paradox^{45,46} which has been first predicted for traffic networks.⁴⁷

It is noted that the existence of cycles is a necessary condition for this paradoxical behavior in oscillator networks. A fundamental example of Braess' paradox was investigated in Ref. 30, starting from a chain network which has no cycles and thus shows no frustration and Braess behavior. Then, a single line is added creating a single cycle and necessary conditions being established under which conditions the closing of the cycles induced Braess' paradox.

V. MULTISTABILITY AND THE NUMBER OF FIXED POINTS

The previous examples show that there can be a large number of stable fixed points in a cyclic network. In the following, we derive conditions for the existence and bounds for the number of stable fixed points depending on the network structure. We start with a deeper analysis of the dynamic condition for arbitrary networks, which is a necessary prerequisite for the existence of a stable fixed point. Then, we turn to the geometric condition and derive bounds for the number of fixed points. The arguments depend heavily on the network structure such that we will start with trees and simple cycles before we turn to more complex topologies.

A. The dynamic condition

We first analyze whether the dynamic condition (13) admits a solution. The problem reduces to the Multi-source multi-sink maximum flow problem, which can be solved by a variety of different algorithms.^{48,49}

So, let $G = (V, E)$ be a connected graph with N nodes and L edges. Each edge is assigned a capacity given by K_1, \dots, K_L , and each node has an in- or outflux given by P_1, \dots, P_N . We define an extended graph $G' = (V', E')$, illustrated in Fig. 3, by adding two vertices s and t to the vertex set,

$$V' = V \cup \{s, t\}, \tag{50}$$

and adding directed links connecting $s(t)$ to all nodes with positive (negative) power injection

$$E = E \cup \{(s \rightarrow j) | j \in V, P_j \geq 0\} \cup \{(j \rightarrow t) | j \in V, P_j < 0\}. \tag{51}$$

The capacity of the newly added links is infinite. Then, one finds the theorem:

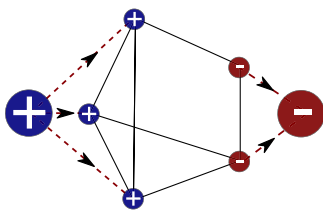


FIG. 3. Illustration of Theorem 9. The original network G (smaller nodes and solid edges) admits solution to the dynamic condition if and only if the extended graph G' with a super source s (big blue node) and a super sink t (big red node) admits an s - t flow larger than the sum of all positive input powers in G .

Theorem 9. A solution of the dynamic condition (13) exists if and only if the value of the maximum s - t -flow \mathcal{F}_{st} in the network G' is larger than or equal to the cumulated input power

$$\mathcal{F}_{st} \geq \sum_{j \in V, P_j \geq 0} P_j. \tag{52}$$

Alternatively, a sufficient condition for the existence of a solution can be found by dividing the graph into parts: let (V_1, V_2) be an arbitrary partition of V and $E(V_1, V_2)$ the cut-set induced by this partition (see Fig. 4). Then, we define

$$\bar{P}_1 = \sum_{v_j \in V_1} P_{v_j}, \quad \bar{P}_2 = \sum_{v_j \in V_2} P_{v_j}, \quad \bar{K}_{12} = \sum_{e \in E(V_1, V_2)} K_e. \tag{53}$$

We note that have assumed that $\sum_j P_j = 0$, without loss of generality, such that we always have $\bar{P}_1 + \bar{P}_2 = 0$.

Theorem 10. If for all partitions (V_1, V_2) we have

$$|\bar{P}_1| = |\bar{P}_2| \leq \bar{K}_{12}, \tag{54}$$

then there exists a solution of the dynamic condition (13).

Proof. The idea is to prove the following:

(\nexists a solution of the dynamic condition (13a) and (13b).

\iff All solutions of (13a) violate (13b)).

$\implies \exists$ a partition (V_1, V_2) with $|\bar{P}_1| \geq \bar{K}_{12}$.

Reversing arguments then yields the theorem. It remains to show that the statement " \implies " is true.

Let F be a solution of (13a). According to our assumption, the set of overloaded edges

$$E_{ov} = \{e \in E | |F_e| > K_e\} \tag{55}$$

is not empty. Now, consider one overloaded edge $e_0 = (u, v) \in E_{ov}$. We assume without loss of generality that the flow is from u to v , i.e., $F_{v,u} > K_{v,u} > 0$. We define the weighted directed network $\tilde{G}(V, \tilde{E})$ with $\tilde{E} = E \setminus e_0$ and coupling constants

$$W_{j,i} = \max\{0, K_{j,i} - F_{j,i}\}. \tag{56}$$

We determine the maximum flow pattern $\Delta F_e, e \in \tilde{E}$ with the value ΔF_{\max} from u to v in the network \tilde{G} . According to the max-flow min-cut theorem, there is a partition (V_1, V_2) with $u \in V_1$ and $v \in V_2$ and the associated cutset $\tilde{E}(V_1, V_2)$ such that

$$\Delta F_e = W_e \quad \text{for all } e \in \tilde{E}(V_1, V_2). \tag{57}$$

Now, consider the flow pattern F' defined by

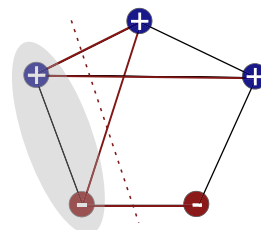


FIG. 4. Illustration of Theorem 10. For each partition of the node set of a graph into V_1 (shaded grey) and V_2 , the induced cutset (edges coloured red) must have capacity not less than the absolute value of input power in V_1 or V_2 .

$$\begin{aligned}\varpi_c &= \frac{1}{2\pi} \sum_{e=1}^L z_e^c \arcsin\left(\frac{F_e}{K_e}\right) \\ &= \frac{1}{2\pi} \sum_{e=1}^L z_e^c \arcsin\left(\frac{F_e^{(0)} + \sum_{c' \in B_C} f_{c'} z_{e'}^{c'}}{K_e}\right),\end{aligned}\quad (66)$$

using Eq. (16). The concept of winding numbers is particularly useful when they are unique. If we can find upper and lower bounds for ϖ_c , then we can simply count the number of solutions $\varpi \in \mathbb{Z}^{L-N+1}$ to obtain the number of fixed points. Uniqueness is rigorously shown for planar graphs in the following lemma.

A graph is called planar if it can be drawn in the plane without any edge crossings. Such a drawing is called a plane graph or a planar embedding of the graph, and any cycle that surrounds a region without any edges is called a face of the graph.³⁵ For the sake of simplicity, we adopt the convention that for plane graphs, the cycle basis B_C is built up from the faces in the following. Notably, many power grids and other supply networks are actually planar. Crossing of power lines is not forbidden *a priori* but is rare.

Lemma 3. *For a planar network, let θ and θ' be two fixed points satisfying the “normal operation” criterion (9). If $\varpi(\theta) = \varpi(\theta')$, then both fixed points are the same, i.e., the phases differ only by an additive constant*

$$\theta = \theta' + c(1, 1, \dots, 1)^T. \quad (67)$$

In other words, no two different fixed points in planar networks can have an identical winding vector.

Proof. Choose as the cycle basis B_C the faces of the plane embedding. The two fixed points can differ only via cycle flows such that the flows can be written as

$$\text{fixed point } \theta: \quad F_e = F_e^{(0)} + \sum_{c \in B_C} f_c z_e^c, \quad (68)$$

$$\text{fixed point } \theta': \quad F'_e = F_e^{(0)} + \sum_{c \in B_C} f'_c z_e^c, \quad (69)$$

defining two cycle flow vectors f and f' . We write $\varpi(f')$ and $\varpi(f)$ in short-hand notation for the corresponding winding vectors. We show that $\varpi(f') = \varpi(f)$ implies $f' = f$ and thus $F' = F$. As we are assuming normal operation, we can reconstruct the phases via (18) and thus find $\theta = \theta' + c(1, 1, \dots, 1)^T$ as we need to show.

So, assume that $\varpi(f') = \varpi(f)$ and $f'_c \neq f_c$ for at least one cycle c . We show that this leads to a contradiction such that the lemma follows. First, consider the case that $f'_c - f_c$ is the same for all cycles: $f'_c - f_c = \Delta f \neq 0$ for all $c \in B_C$. Then, choose a cycle k at the boundary. If $\Delta f > 0$, we find $\varpi_k(f') > \varpi_k(f)$, and if $\Delta f < 0$, we find $\varpi_k(f') < \varpi_k(f)$. This contradicts the assumption and the lemma follows.

Otherwise, choose a cycle for which the quantity $f'_c - f_c$ is the largest. We can find a cycle k such that

$$f'_k - f_k \geq f'_\ell - f_\ell \quad \text{for all } \ell \neq k, \quad (70)$$

$$f'_k - f_k > f'_n - f_n \quad \text{for at least one cycle } n \text{ adjacent to } k. \quad (71)$$

or, equivalently,

$$f'_k - f'_\ell \geq f_k - f_\ell \quad \text{for all } \ell \neq k, \quad (72)$$

$$f'_k - f'_n > f_k - f_n \quad \text{for at least one cycle } n \text{ adjacent to } k. \quad (73)$$

We now exploit that any edge belongs to at most two cycles, according to Mac Lane’s planarity criterion.⁵⁰ Choosing an edge e which is part of both the cycles k and n , we have $z_e^k z_e^k = 1$ and $z_e^k z_e^n = -1$. For all other cycles $\ell \neq k, n$, we have $z_e^\ell = 0$. Thus, we find [using (73)]

$$\begin{aligned}z_e^k F_e^{(0)} + \underbrace{z_e^k z_e^k f'_k}_{=+1} + \underbrace{z_e^k z_e^n f'_n}_{=-1} + \sum_{\ell \neq k, n} \underbrace{z_e^k z_e^\ell f'_\ell}_{=0} &> z_e^k F_e^{(0)} \\ + \underbrace{z_e^k z_e^k f_k}_{=+1} + \underbrace{z_e^k z_e^n f_n}_{=-1} + \sum_{\ell \neq k, n} \underbrace{z_e^k z_e^\ell f_\ell}_{=0},\end{aligned}\quad (74)$$

$$\rightarrow z_e^k F_e^{(0)} + \sum_c z_e^k z_e^c f'_c > z_e^k F_e^{(0)} + \sum_c z_e^k z_e^c f_c. \quad (75)$$

For every other edge e' in cycle k , we find by the same procedure [using (72)] that

$$z_{e'}^k F_{e'}^{(0)} + \sum_c z_{e'}^k z_e^c f'_c \geq z_{e'}^k F_{e'}^{(0)} + \sum_c z_{e'}^k z_e^c f_c. \quad (76)$$

Substituting these two inequalities in the definition (66) and using that arcsin is monotonically increasing and point-symmetric about the origin such that $\arcsin(z_e^k x) = z_e^k \arcsin(x)$, we find

$$\varpi_k(f') > \varpi_k(f). \quad (77)$$

This contradicts our contrary assumption, which concludes the proof. \square

We note that Delabays *et al.* have proved this lemma using completely different techniques in Ref. 51.

D. Simple cycles

For networks containing a single cycle (a ring network), tight upper and lower bounds can be obtained for the number of fixed points satisfying $\cos(\theta_i^* - \theta_j^*) > 0$ for all edges (i, j) . These states correspond to the normal operation of a power grid and are guaranteed to be stable by corollary 1. Other stable steady states can exist in particular at the border of the stable parameter region.²⁹ We label the nodes as $1, 2, \dots, N$ along the cycle, fixing the direction of counting in the counter-clockwise direction and identify node 1 with $N+1$ and 0 with N . Likewise, we fix the orientation of the edges $e \in \{1, \dots, L\}$ such that $F_e > 0$ describes a counter-clockwise flow and $F_e < 0$ a clockwise flow.

We will first calculate the exact number of fixed points counting the number of different allowed winding numbers. However, this result depends on one particular solution of the dynamic conditions (11), thereby limiting its applicability. We therefore also derive lower and upper bounds for the number of fixed points in terms of a few simple characteristics of the grid, in particular, the maximum partial net power. These bounds do not depend on any particular solution of the dynamical condition.

Remark 11. For any ring network \mathcal{R}_N with N nodes, the cycle flow vector defined in (2) and the winding vector defined in (29) naturally reduce into single numbers. We refer to them as cycle flow f_c and winding number ϖ_c , following Ref. 39. These two quantities will be crucial in establishing the results in the rest of this section.

Theorem 12. For a ring network \mathcal{R}_N , the number of normal operation fixed points (denoted by \mathcal{N}) is given by

$$\mathcal{N} = \left\lceil \frac{1}{2\pi} \sum_j \arcsin \left(\frac{F_{j+1,j}^{(0)} + f_c^{\max}}{K_{j+1,j}} \right) \right\rceil - \left\lfloor \frac{1}{2\pi} \sum_j \arcsin \left(\frac{F_{j+1,j}^{(0)} + f_c^{\min}}{K_{j+1,j}} \right) \right\rfloor - 1, \quad (78)$$

where $\lfloor \cdot \rfloor$ denotes the floor function and $\lceil \cdot \rceil$ denotes the ceiling function. $F_{ij}^{(0)}$ is one particular solution to the dynamic condition (11) and

$$\begin{aligned} f_c^{\max} &= \min_j (K_{j+1,j} - F_{j+1,j}^{(0)}), \\ f_c^{\min} &= \max_j (-K_{j+1,j} - F_{j+1,j}^{(0)}). \end{aligned} \quad (79)$$

Proof. Suppose that we have one fixed point θ_0 with the flows $F_{ij}^{(0)}$ and analyze (as per Theorem 3) which cycle flow values f_c lead to different valid fixed points. First, the cycle flow bounds both above and below since the flow $F_{j,j+1}$ along each edge cannot exceed in absolute value the capacity $K_{j,j+1}$

$$f_c^{\min} < f_c < f_c^{\max}, \quad (80)$$

$$f_c^{\max} = \min_j (K_{j,j+1} - F_{j,j+1}^{(0)}), \quad (81)$$

$$f_c^{\min} = \max_j (-K_{j,j+1} - F_{j,j+1}^{(0)}). \quad (82)$$

We emphasize that f_c cannot be equal to f_c^{\max} or f_c^{\min} because otherwise one edge would be fully loaded with $\cos(\theta_i - \theta_j) = 0$, contradicting our assumption.

Second, all fixed points have to satisfy the geometric condition (cf. Theorem 7)

$$\varpi(f_c) \in \mathbb{Z}. \quad (83)$$

Since we restrict ourselves to normal operation, the winding number for a single cycle reads

$$\varpi(f_c) = \frac{1}{2\pi} \sum_j \arcsin \left(\frac{F_{j+1,j}^{(0)} + f_c}{K_{j+1,j}} \right). \quad (84)$$

Using the bound for the cycle flow strength (80) and the fact that arcsin is a monotonically increasing function, we find that the winding number is also bound by

$$\varpi(f_c^{\min}) \leq \varpi \leq \varpi(f_c^{\max}). \quad (85)$$

As the winding numbers are unique (see Lemma 3), the distinct fixed points correspond to the following values of the winding number:

$$\varpi_{\text{fixedpoint}} = \lfloor \varpi(f_c^{\min}) \rfloor + 1, \lfloor \varpi(f_c^{\min}) \rfloor + 2, \dots, \lceil \varpi(f_c^{\max}) \rceil - 1. \quad (86)$$

Counting these values and inserting the values of f_c^{\min} and f_c^{\max} then yield the number of fixed points \mathcal{N} . \square

For practical applications, it is desirable to determine the number of fixed points from the properties of the network alone, without referring to a particular solution $F^{(0)}$. To obtain suitable bounds for the number of fixed points \mathcal{N} , we first define some properties which characterize the network.

Definition 13. For a ring network \mathcal{R}_N with $N \in \mathbb{N}$ nodes indexed by $1, 2, \dots, N$ along the cycle, a **fragment** \mathcal{F}_{ij} is defined as the path starting at node i and ending at node j . For any fragment \mathcal{F}_{ij} , the **partial net power** \bar{P}_{ij} is defined as

$$\bar{P}_{ij} = \sum_{k=i}^j P_k. \quad (87)$$

and the **maximal partial net power** is defined as

$$\bar{P}_{\max} = \max_{i,j} \bar{P}_{ij}. \quad (88)$$

This concept is illustrated in Fig. 5. Furthermore, we define the maximum and minimum transmission capacities

$$K_{\max} = \max_j K_{j+1,j} \quad \text{and} \quad K_{\min} = \min_j K_{j+1,j}. \quad (89)$$

Lemma 4. For any ring fragment \mathcal{F}_{ij} , the partial net power is equal to the net outward flow

$$\bar{P}_{ij} = F_{j+1,j} - F_{i-1,i} \quad (90)$$

and

$$\bar{P}_{\max} = \max_j F_{j+1,j} - \min_i F_{i-1,i}. \quad (91)$$

Lemma 4 is a formalization of energy conservation. The net outward flow from a segment must equal the cumulated power injections in the fragment. We then seek the fragment maximizing the total flow exchanged with the rest of the ring. We note that the definitions of \bar{P}_{ij} and \bar{P}_{\max} appeared previously in Ref. 51.

Corollary 3. For a ring network \mathcal{R}_N , the number of normal operation fixed points (denoted by \mathcal{N}) is bound from above and below by

$$0 \leq \mathcal{N} \leq 2 \left\lfloor \frac{N}{4} \right\rfloor + 1 \quad (92)$$

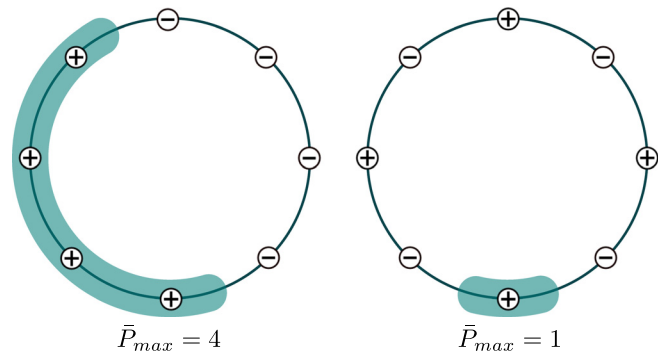


FIG. 5. The maximum partial net power \bar{P}_{\max} in different ring networks.

and by

$$\left\lceil \frac{N}{4} \frac{2K_{\max} - \bar{P}_{\max}}{K_{\min}} \right\rceil \geq \mathcal{N} \geq \left\lfloor \frac{N}{2\pi} \frac{2K_{\min} - \bar{P}_{\max}}{K_{\max}} \right\rfloor - 1. \quad (93)$$

Proof. According to Lemma 12, the number of fixed points \mathcal{N} is given by

$$\mathcal{N} = \lceil \varpi(f_c^{\max}) \rceil - \lfloor \varpi(f_c^{\min}) \rfloor - 1. \quad (94)$$

We make use of the fact that the arcsin function is bound, $\arcsin(x) \in [-\pi/2, +\pi/2]$, such that

$$\begin{aligned} \varpi(f_c^{\max}) &= \frac{1}{2\pi} \sum_{j=1}^N \arcsin\left(\frac{F_{j+1,j}^{(0)} + f_c^{\max}}{K_{j+1,j}}\right) < \frac{N}{4}, \\ \varpi(f_c^{\min}) &= \frac{1}{2\pi} \sum_{j=1}^N \arcsin\left(\frac{F_{j+1,j}^{(0)} + f_c^{\min}}{K_{j+1,j}}\right) > -\frac{N}{4}. \end{aligned} \quad (95)$$

This proves the first part (92) of the corollary. To prove the second part, we start from

$$\lceil \varpi(f_c^{\max}) - \varpi(f_c^{\min}) \rceil - 1 \leq \mathcal{N} \leq \lceil \varpi(f_c^{\max}) - \varpi(f_c^{\min}) \rceil. \quad (96)$$

Now, one can obtain upper and lower bounds for all terms in the sum using the trigonometric relation

$$x - y \leq \arcsin(x) - \arcsin(y) \leq \frac{\pi}{2}(x - y), \quad (97)$$

which holds for all $-1 \leq y \leq x \leq 1$. This yields

$$\frac{1}{2\pi} \sum_j \frac{\Delta f_c}{K_{j+1,j}} \leq \varpi(f_c^{\max}) - \varpi(f_c^{\min}) \leq \frac{1}{4} \sum_j \frac{\Delta f_c}{K_{j+1,j}}, \quad (98)$$

where we define $\Delta f_c = f_c^{\max} - f_c^{\min}$. Furthermore, this quantity can be bound as

$$\begin{aligned} \Delta f_c &= \min_j (K_{j+1,j} - F_{j+1,j}^{(0)}) - \max_j (-K_{j+1,j} - F_{j+1,j}^{(0)}) \\ &\geq 2K_{\min} + \min_j (-F_{j+1,j}^{(0)}) - \max_j (-F_{j+1,j}^{(0)}), \\ &= 2K_{\min} + \max_j (F_{j,j+1}^{(0)}) - \max_j (-F_{j+1,j}^{(0)}), \\ &= 2K_{\min} - \bar{P}_{\max} \quad (\text{using (92)}), \end{aligned} \quad (99)$$

such that the fraction in Eq. (98) becomes

$$\frac{\Delta f_c}{K_{j+1,j}} \geq \frac{2K_{\min} - \bar{P}_{\max}}{K_{\max}}. \quad (100)$$

In a similar way, we find

$$\Delta f_c \leq 2K_{\max} - \bar{P}_{\max}. \quad (101)$$

Substituting these bounds into Eq. (98) yields

$$\begin{aligned} \varpi(f_c^{\max}) - \varpi(f_c^{\min}) &\geq \frac{N}{2\pi} \frac{2K_{\min} - \bar{P}_{\max}}{K_{\max}}, \\ \varpi(f_c^{\max}) - \varpi(f_c^{\min}) &\leq \frac{N}{4} \frac{2K_{\max} - \bar{P}_{\max}}{K_{\min}}, \end{aligned} \quad (102)$$

which combined with (96) completes the proof. \square

We note that the first part of this bound (92) had previously been shown by Ochab and Gora³⁸ as well as by Delabays *et al.*³⁷

Corollary 4. For homogeneous rings \mathcal{R}_N , i.e., $K_{i,i+1} = K$, Eq. (93) simplifies to

$$\left\lfloor \frac{N}{\pi} - \frac{N\bar{P}_{\max}}{2K\pi} \right\rfloor - 1 \leq \mathcal{N} \leq \left\lfloor \frac{N}{2} - \frac{N\bar{P}_{\max}}{4K} \right\rfloor. \quad (103)$$

In particular, ring networks \mathcal{R}_N with $N \leq 4$ do not have multiple stable fixed points. Ring network \mathcal{R}_N with $N \geq 7$ nodes will have multiple stable fixed points ($\mathcal{N} \geq 2$) if

$$\bar{P}_{\max} < 2K_{\min} - \frac{4\pi}{N} K_{\max}. \quad (104)$$

These relations can be proven by simply evaluating the bounds in Corollary 3.

Corollary 5. As K is decreased in a homogeneous ring network, the fixed points with the largest infinity norm of the flows

$$\|\mathbf{F}\|_{\infty} := \max_j |F_{j,j+1}|$$

will be the first ones to vanish.

Proof. We can see from (95) that both $\varpi(f_c^{\max})$ and $\varpi(f_c^{\min})$ are monotonically increasing functions of f_c^{\max} and f_c^{\min} , respectively. According to (80), when K is decreased, f_c^{\max} decreases and f_c^{\min} increases. The corollary follows. \square

We illustrate how the bounds scale with the connectivity K and \bar{P}_{\max} for a sample ring of size $N = 16$ in Fig. 6. We see in Fig. 6(a) that increasing K results in more stable fixed points. Whereas Fig. 6(b) demonstrates that if the power generators ($P_j \geq 0$) are clustered together, then the system has less fixed points, as opposed to the case where they are more distributed.

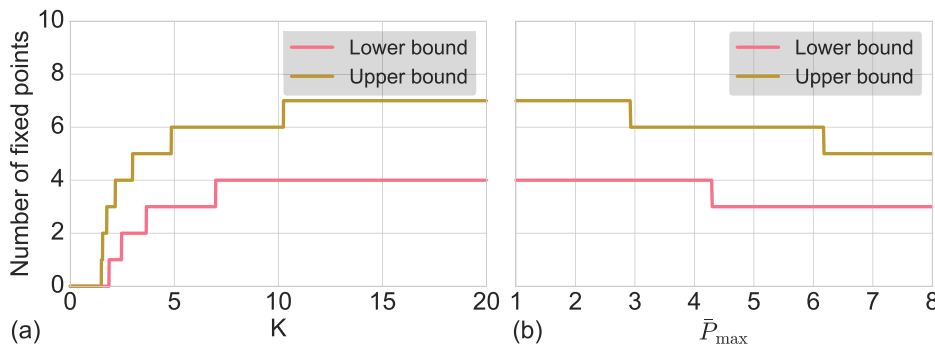


FIG. 6. Upper and lower bounds for the number of fixed points \mathcal{N} for a sample 16 element ring as a function of (a) $K = K_{j,j+1}$ for all $1 \leq j \leq 16$ at $\bar{P}_{\max} = 3$ and (b) \bar{P}_{\max} at $K = 10$.

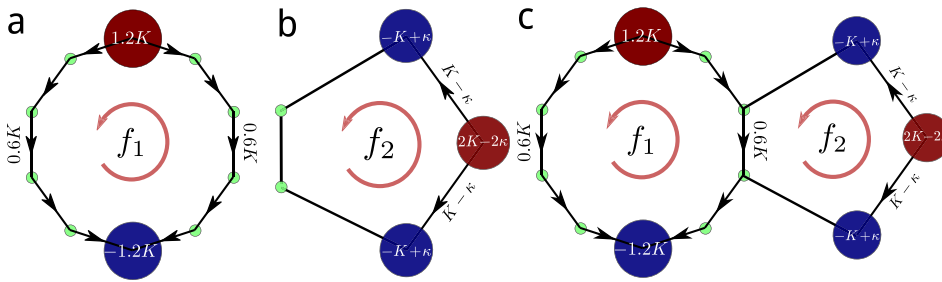


FIG. 7. Difficulties in finding bound for the number of stable fixed points in the complex network. The network motifs shown in (a) and (b) have 3 and 1 stable fixed points, respectively, whereas the fused network shown in (c) has no stable fixed point at all. The power injections P_j are given in the nodes. All edges have transmission capacity K .

E. Complex networks

Obtaining bounds for the number of fixed points is hard in general, as we cannot simply decompose a network into single cycles, unless no two cycles of a network share an edge. The difficulty arises because cycle flows in two faces sharing one or more edges can cancel or enhance each other. This is why one cannot simply multiply the bounds for a number of fixed points for each cycle to obtain a bound for the total number of fixed points for a network. We demonstrate this using two examples.

1. Two cycle flows destroying each other

First, we show that even if all single cycles support (multiple) fixed points in case they are isolated, the full network may not have a single fixed point at all. This is illustrated in Fig. 7 for a network consisting of just two cycles. The network motifs shown in panels (a) and (b) have 3 and 1 stable fixed points, respectively, whereas the full network shown in panel (c) does not have a stable fixed point. Isolated cycle 2, i.e., the network shown in Fig. 7(b), has a stable fixed point, but two edges are heavily loaded such that there is nearly no security margin and no available capacity for cycle flows. Fusing the two cycles as in Fig. 7(c) disturbs the geometric condition for both cycles. To restore the geometric condition $\varpi \in \mathbb{Z}^2$, we would have to add some cycle flows. But this is impossible in cycle 2 such that there is no stable fixed point in the full network.

2. Two cycle flows getting created

So, we have seen that getting a lower bound for a number of fixed points of a general network is hard, as multiplying lower bounds for each cycle in a cycle basis does not yield a valid lower bound. Next, we will show why obtaining a good upper bound is also hard.

Consider any of the two identical single loop networks in Fig. 8. It consists of one generator and one consumer, generating and consuming $2.1K$ power, respectively. Each edge has capacity K . None of the two single loop networks have any fixed point: simply because the network does not have enough capacity to transport the $2.1K$ amount of power from the

generator to the consumer. However, when those two are fused together, two cycle flows emerge and a stable fixed point with winding vector $\omega = (1, -1)$ comes into existence. This should not come as a surprise: fusing two cycles in this case ended up with an alternate pathway for the powerflow being created.

F. Planar networks

Although obtaining estimates for a number of fixed points for general topologies is quite difficult, we now show that for planar topologies, it is possible to obtain some analytical insights.

1. Upper bound

Theorem 14. Consider a finite planar network. Choose the faces of the graph as the cycle basis B_C . Then, the number of normal operation fixed points, i.e., fixed points satisfying $\cos(\theta_i^* - \theta_j^*) > 0$ for all edges (i, j) , is bound from above by

$$\mathcal{N} < \prod_{c=1}^{L-N+1} 2 \left\lfloor \frac{N_c}{4} \right\rfloor + 1, \tag{105}$$

where N_c is the number of nodes in cycle c .

Proof. In a planar network, no two different fixed points can have the same winding vector ϖ (see Lemma 3) such that we can just count the different allowed winding vectors. For each fundamental cycle $c \in B_C$, we have

$$- \lfloor N_c/4 \rfloor < \varpi_c = \frac{1}{2\pi} \sum_{e \in \text{cycle } c} \Delta_e < + \lfloor N_c/4 \rfloor \tag{106}$$

because $-\pi/2 < \Delta_e < +\pi/2$ in normal operation. Counting the number of different possible values of the winding numbers $\varpi_1, \dots, \varpi_{L-N+1}$ respecting these upper and lower bounds yields the result. \square

Delabays *et al.* have presented³⁷ this bound in the case of uniform power injections P_j at all nodes. They have also determined topological conditions that are sufficient to ensure that all fixed points are under normal operation, thus making the upper bound in (105) valid for all fixed points in a certain class of networks.

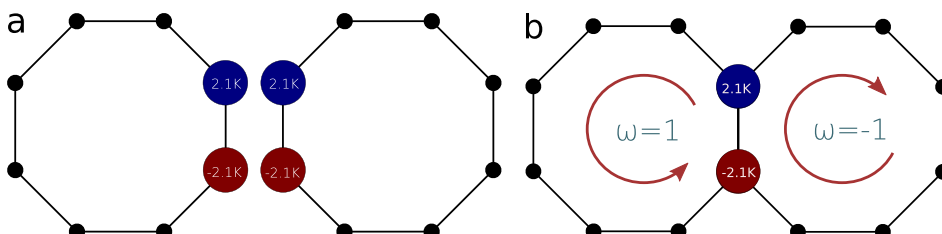


FIG. 8. Two ring networks, each with no fixed point, when merged by an edge, gain a fixed point.

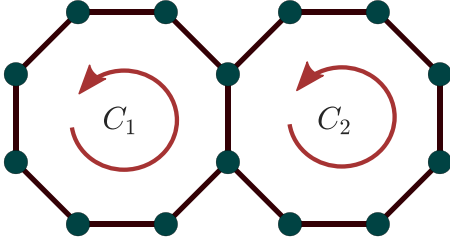


FIG. 9. A 2-cycle network. We use the convention that cycles are counter-clockwise. Therefore, we assign positive magnitudes to counter-clockwise cycle flows and negative magnitudes to clockwise cycle flows.

Intriguingly, this upper bound has been demonstrated to be *invalid*⁵¹ outside normal operation.

2. Asymptotic behaviour

We have shown in Subsection V E that it is not straightforward to obtain bounds for the number of fixed points \mathcal{N} in complex networks, unlike simple cycles. However, in the limit of $N \gg 1, K \gg 1$, we can nevertheless derive the scaling behaviour for \mathcal{N} .

3. Two-cycle network

For simplicity, we first consider a network with homogeneous transmission capacities consisting of two cycles C_1 and C_2 , as illustrated in Fig. 9. Suppose that there are n_1 edges belonging only to cycle 1, n_2 edges belonging only to cycle 2

and n_{12} edges belonging to both. Let one fixed point be θ^* with flows in each cycle and the intersection be bound by

$$F_1^{\min} \leq F_e \leq F_1^{\max}, \quad \text{for all } e \in C_1 - C_2 \quad (107)$$

$$F_2^{\min} \leq F_e \leq F_2^{\max}, \quad \text{for all } e \in C_2 - C_1 \quad (108)$$

$$F_{12}^{\min} \leq F_e \leq F_{12}^{\max}, \quad \text{for all } e \in C_2 - C_1. \quad (109)$$

Then, the possible cycle flows in each cycle are bound inside a convex polygon \mathcal{D} described by

$$-K - F_1^{\min} \leq f_1 \leq K - F_1^{\max}, \quad (110)$$

$$-K - F_2^{\min} \leq f_2 \leq K - F_2^{\max}, \quad (111)$$

$$-K - F_{12}^{\min} \leq f_1 - f_2 \leq K - F_{12}^{\max}. \quad (112)$$

Then, for $K \gg 1, n_1 \gg 1, n_2 \gg 1$, the number of fixed points converges to the area of the image set of \mathcal{D} under the mapping ϖ .

$$\mathcal{N} \approx \int_{\varpi(\mathcal{D})} d\varpi_1 d\varpi_2, \quad (113)$$

$$= \int_{\mathcal{D}} df_1 df_2 \det J(\varpi), \quad (114)$$

where the Jacobian $J(\varpi)$ for the change in the variable can be computed from the expression for ϖ in (66), which yields

$$\det J(\varpi) = \frac{1}{4K^2\pi^2} \times \det \begin{pmatrix} \sum_{e \in C_1} \frac{1}{\sqrt{1 - \left(\frac{F_e + f_1}{K}\right)^2}} + \sum_{e \in C_1 \cap C_2} \frac{1}{\sqrt{1 - \left(\frac{F_e + f_1 - f_2}{K}\right)^2}} - \sum_{e \in C_1 \cap C_2} \frac{1}{\sqrt{1 - \left(\frac{F_e + f_1 - f_2}{K}\right)^2}} \\ - \sum_{e \in C_1 \cap C_2} \frac{1}{\sqrt{1 - \left(\frac{F_e + f_1 - f_2}{K}\right)^2}} & \sum_{e \in C_2} \frac{1}{\sqrt{1 - \left(\frac{F_e + f_2}{K}\right)^2}} + \sum_{e \in C_1 \cap C_2} \frac{1}{\sqrt{1 - \left(\frac{F_e + f_1 - f_2}{K}\right)^2}} \end{pmatrix}. \quad (115)$$

Taking the limits

$$\begin{aligned} \lim_{K \rightarrow \infty} \frac{F_e + f_1}{K} &= \frac{f_1}{K}, \\ \lim_{K \rightarrow \infty} \frac{F_e + f_2}{K} &= \frac{f_2}{K}, \end{aligned} \quad (116)$$

leads to

$$\mathcal{N} \approx \frac{1}{4K^2\pi^2} \int_{\tilde{\mathcal{D}}} df_1 df_2 \det \begin{pmatrix} \frac{n_1}{\sqrt{1 - \left(\frac{f_1}{K}\right)^2}} + \frac{n_{12}}{\sqrt{1 - \left(\frac{f_1 - f_2}{K}\right)^2}} & - \frac{n_{12}}{\sqrt{1 - \left(\frac{f_1 - f_2}{K}\right)^2}} \\ - \frac{n_{12}}{\sqrt{1 - \left(\frac{f_1 - f_2}{K}\right)^2}} & \frac{n_2}{\sqrt{1 - \left(\frac{f_2}{K}\right)^2}} + \frac{n_{12}}{\sqrt{1 - \left(\frac{f_1 - f_2}{K}\right)^2}} \end{pmatrix}. \quad (117)$$

$$\tilde{\mathcal{D}} : = \{(f_1, f_2) : (f_1, f_2) \in \mathbb{R}^2, |f_1| \leq K, |f_2| \leq K, |f_1 - f_2| \leq K\}.$$

Redefining $f_1 \rightarrow f_1/K, f_2 \rightarrow f_2/K$, we obtain

$$\mathcal{N} \approx \frac{1}{4\pi^2} \int_{\mathcal{D}} df_1 df_2 \det \begin{pmatrix} \frac{n_1}{\sqrt{1-f_1^2}} + \frac{n_{12}}{\sqrt{1-(f_1-f_2)^2}} & -\frac{n_{12}}{\sqrt{1-(f_1-f_2)^2}} \\ -\frac{n_{12}}{\sqrt{1-(f_1-f_2)^2}} & \frac{n_2}{\sqrt{1-f_2^2}} + \frac{n_{12}}{\sqrt{1-(f_1-f_2)^2}} \end{pmatrix}, \tag{118}$$

$$= \frac{1}{4\pi^2} \left(n_1 n_2 \int_{\mathcal{D}} \frac{1}{\sqrt{1-f_1^2}} \frac{1}{\sqrt{1-f_2^2}} df_1 df_2 + n_1 n_{12} \int_{\mathcal{D}} \frac{1}{\sqrt{1-f_1^2}} \frac{1}{\sqrt{1-(f_1-f_2)^2}} df_1 df_2 \right. \\ \left. + n_2 n_{12} \int_{\mathcal{D}} \frac{1}{\sqrt{1-f_2^2}} \frac{1}{\sqrt{1-(f_1-f_2)^2}} df_1 df_2 \right), \tag{119}$$

$$= \frac{1}{4\pi^2} \left(n_1 n_2 \int_{\mathcal{D}} \frac{1}{\sqrt{1-f_1^2}} \frac{1}{\sqrt{1-f_2^2}} df_1 df_2 + (n_1 + n_2) n_{12} \int_{\mathcal{D}} \frac{1}{\sqrt{1-f_1^2}} \frac{1}{\sqrt{1-(f_1-f_2)^2}} df_1 df_2 \right). \tag{120}$$

In the last line, we use the symmetry in f_1 and f_2 , both in the integrand and the domain of integration. We can simplify even further, by using the following change in variables:

$$(f_1, f_2) \mapsto (f_2 - f_1, f_2).$$

We note that the domain remains the same after this change in the variable and the determinant of the Jacobian $\det(J) = -1$. This allows the simplification

$$\mathcal{N} \approx (n_1 n_2 + (n_1 + n_2) n_{12}) \underbrace{\frac{1}{4\pi^2} \int_{\mathcal{D}} \frac{1}{\sqrt{1-f_1^2}} \frac{1}{\sqrt{1-f_2^2}} df_1 df_2}_{\gamma}$$

with

$$\begin{aligned} \gamma &= \frac{1}{4\pi^2} \left\{ \int_{-1}^0 \frac{df_1}{\sqrt{1-f_1^2}} \int_{-1}^{f_1+1} \frac{df_2}{\sqrt{1-f_2^2}} + \int_0^1 \frac{df_1}{\sqrt{1-f_1^2}} \int_{f_1-1}^1 \frac{df_2}{\sqrt{1-f_2^2}} \right\}, \\ &= \frac{1}{4\pi^2} \left\{ \int_{-1}^0 \frac{\arcsin(f_1 + 1) + \frac{\pi}{2}}{\sqrt{1-f_1^2}} df_1 + \int_0^1 \frac{\frac{\pi}{2} - \arcsin(f_1 - 1)}{\sqrt{1-f_1^2}} df_1 \right\}, \\ &= \frac{1}{4\pi^2} \left\{ \frac{\pi^2}{4} + \int_{-1}^0 \frac{\arcsin(f_1 + 1)}{\sqrt{1-f_1^2}} df_1 + \frac{\pi^2}{4} + \int_0^1 \frac{\arcsin(f_1 - 1)}{\sqrt{1-f_1^2}} df_1 \right\}, \\ &= \frac{1}{8} + \frac{1}{2\pi^2} \int_{-1}^0 \frac{\arcsin(f_1 + 1)}{\sqrt{1-f_1^2}} df_1, \\ &\approx 0.1576, \end{aligned}$$

to finally yield this scaling result

$$\lim_{n_1, n_2 \rightarrow \infty} \mathcal{N} = \gamma(n_1 n_2 + (n_1 + n_2) n_{12}), \tag{121}$$

$$\gamma \approx 0.1576.$$

To evaluate the accuracy of (121), we apply it to two special cases. First, we consider networks with $n = n_1 = n_2, n_{12} = 1$, i.e., two identical cycles sharing only one single edge. In this case, (121) becomes

$$\mathcal{N}(n, n, 1) \approx (n^2 + 2n)\gamma. \tag{122}$$

Second, we consider networks with $n = n_1 = n_2, n_{12} = n$, i.e., two identical cycles sharing half of their edges. In this case, (121) becomes

$$\mathcal{N}(n, n, n) \approx 3\gamma n^2. \tag{123}$$

We see in Fig. 10 that in both these cases, the scaling relations are quite accurate even for not very large network sizes, such as $n = 50$.

4. General planar graphs

The scaling results for two-cycle networks can be extended to general planar graphs; to this end, we define a few quantities.

Definition 15 (Loopy dual graph). Given a planar graph $G(V, E)$ and an embedding, we choose a cycle basis B_C consisting of the faces of the embedding. The loopy dual graph $G^{\text{dual}}(G)$ is an undirected multigraph whose vertex set is equal to B_C . Its edge set E' is as follows. For each edge

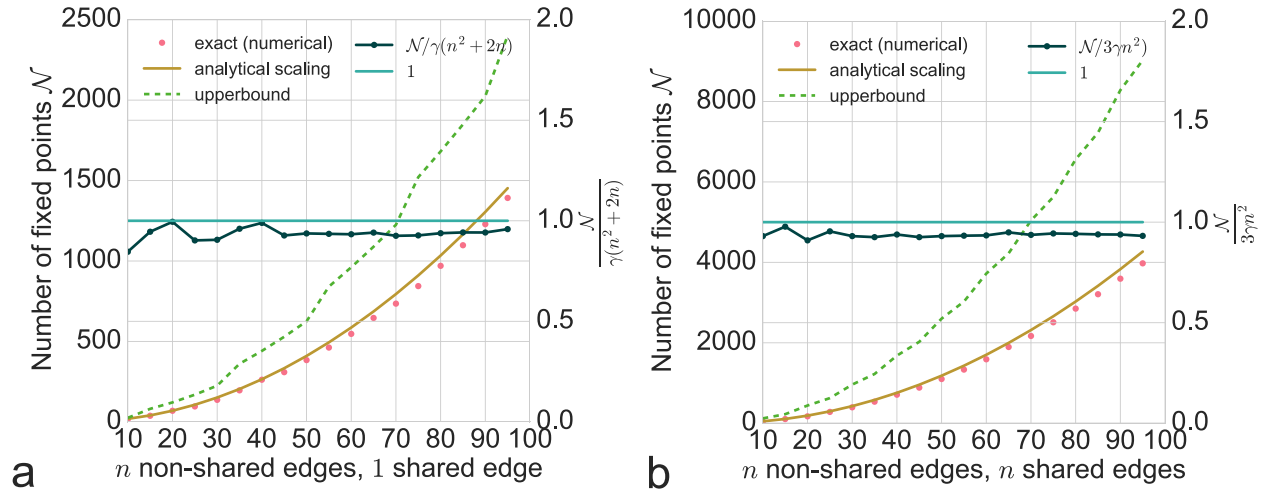


FIG. 10. (a) Scaling of the number of fixed points for two-cycle networks at zero power injection and infinite edge capacity limit. (a) Each cycle has $n + 1$ edges, and they share one edge between them. (Left y-axis) The dots show the exact number of fixed points computed numerically. The solid line shows the predicted number as per scaling relation (121). The dashed line shows the upper bound (105). (Right y-axis) The dotted line shows the number of fixed points divided by $n^2 + 2n$ converging to a constant value, that is close to the analytically predicted value $\gamma = 0.1576$, as per equation (121). (b) The same as (a), but for networks where each cycle has $2n$ edges, they share n edges between them.

$e \in E$, if it is shared between two cycles c_1 and c_2 , then an edge between c and c' is added to E' . If e is at the boundary and belongs to only one cycle c , then a self-loop is added at node c . We illustrate this definition in Fig. 11.

Now, consider a planar graph and an arbitrarily chosen fixed point with flows F_e . Let us denote by \tilde{L}^{loopy} the loopy Laplacian of its metagraph, as defined in Definition 1.

Then, Eq. (117) generalizes to

$$\mathcal{N} \approx \frac{1}{(2K\pi)^{L-N+1}} \int_{\tilde{\mathcal{D}}} df_1 df_2 \cdots df_{L-N+1} \det \tilde{L}^{\text{loopy}}, \quad (124)$$

$$\tilde{\mathcal{D}} := \{(f_1, f_2, \dots, f_{L-N+1}) : |f_i| \leq K, |f_i - f_j| \leq K \text{ if cycles } i, j \text{ share an edge}\}.$$

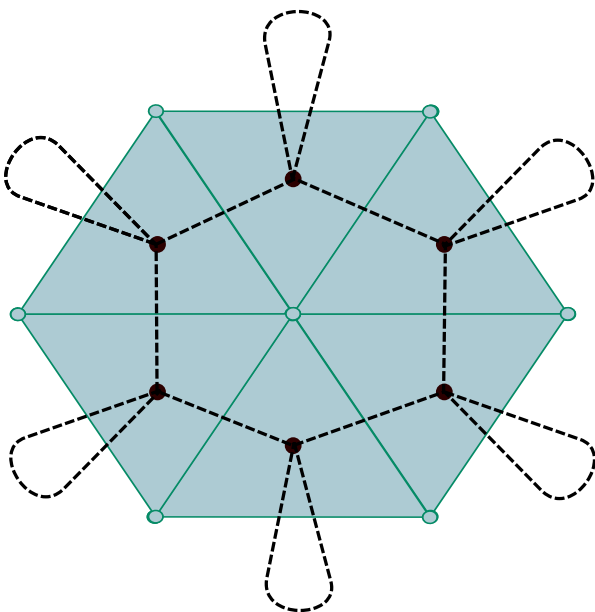


FIG. 11. A planar graph (solid edges, unfilled circular nodes) and its loopy dual (dashed edges, filled circular nodes) corresponding to this specific embedding.

VI. UNSTABLE FIXED POINTS

In principle, we can generalize the cycle flow approach to find fixed points which do not satisfy the normal operation condition, too. These fixed points are typically linearly unstable (cf. the discussion in Ref. 30) However, most of the results on the number of fixed points cannot be generalized to this case. As an instructive example, consider again a homogeneous ring as in Sec. IV C. We label the nodes as $1, 2, \dots, N$ along the cycle and assume that N is an integer multiple of 4. All nodes have a vanishing power injection $P_j \equiv 0$, and all links have an equal strength K as before. Then, it is easy to see that

$$\theta^* = (0, \delta, \pi, \pi + \delta, 2\pi, 2\pi + \delta, 3\pi, \dots)^T \quad (125)$$

is a fixed point of the dynamics for each value of $\delta \in [0, \pi)$. This class of fixed points represents a pure cycle flow

$$F_{j,j+1} = K \sin(\theta_{j+1} - \theta_j) = K \sin(\delta) \quad (126)$$

for all edges $(j, j + 1)$. The winding number is $\varpi = N/4$ independent of the value of δ and the edges belong alternately to E_+ and E_-

$$\begin{aligned} E_+ &= \{(1, 2); (3, 4); (5, 6); \dots\}, \\ E_- &= \{(2, 3); (4, 5); (6, 7); \dots\}. \end{aligned} \quad (127)$$

This simple example shows that two main assumptions made for the normal operation fixed points (where $E_- = \{\}$) do not longer hold: first, the set of fixed points is no longer discrete. Instead, we find a continuum of solutions parametrized by the real number δ . Second, different fixed points yield the same winding number. Thus, we cannot obtain the number of fixed points by counting winding numbers in general.

VII. CALCULATING ALL FIXED POINTS

The cycle flow approach yields a convenient method to calculate multiple fixed points for oscillator networks.

Generally, it is hard to make sure that a numerical algorithm yields all solutions for a nonlinear algebraic equation. However, we have shown that the winding numbers are unique at least for normal operation fixed points in planar networks. Thus, we can scan the allowed values of the winding numbers and try to find a corresponding solution. This can be done by starting from an arbitrary solution of the dynamical condition and adding cycle flows until we obtain the desired winding numbers.

In particular, we can calculate all fixed points in normal operation for a planar network using the following algorithm:

1. Find a solution $F^{(0)}$ of the dynamic condition.
2. Fix a plane embedding and a cycle basis.
3. Vary the number z_c in the interval $[-\frac{N_c}{4}, \frac{N_c}{4}]$, for all cycles $c = 1, \dots, L - N + 1$.
4. Try to solve the set of equations

$$\varpi_c(f) = z_c \quad \text{for all } c = 1, \dots, L - N + 1, \quad (128)$$

where the winding numbers are given by Eq. (27). Dropping the assumption of a normal operation, we lose the guarantee of uniqueness as discussed in Sec. VI. Nevertheless, the method can be readily adapted to find *most*

of the unstable fixed points, at least if the number $|E_-|$ is small. This can be very useful, as a systematic calculation of such fixed points is generally not straightforward. The results can be applied, among other things, to assess the global stability of a stable fixed point by analyzing the stability boundary^{52,53} or the stability in the presence of stochastic fluctuations.⁵⁴ In particular, we must add another step to the algorithm to loop over all possible sets E_- :

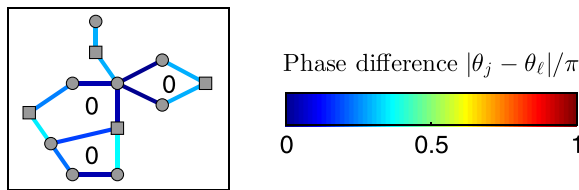
- 3a. Vary $k = 0, \dots, L$. Then, sample all k -tuples from the edge set E to define the set E_- .
- 3b. Vary the number z_c in the interval $[-\frac{N_c}{4}, \frac{N_c}{4}]$, for all cycles $c = 1, \dots, L - N + 1$.

The output of this algorithm is shown in Fig. 12 for a small test network and $|E_-| \leq 2$. For this small network, we have only $L - N + 1 = 3$ fundamental cycles of which one is decoupled. Hence, we can graphically check that we have obtained *all* fixed points.

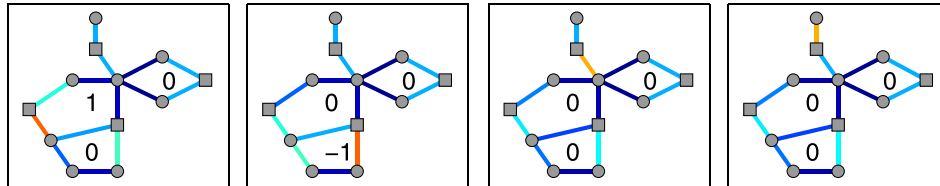
VIII. DISCUSSION

Oscillator networks are ubiquitous in nature and technology. A lot of research in statistical physics starting from

Fixed points with $|E_-| = 0$ (normal operation):



Fixed points with $|E_-| = 1$:



Fixed points with $|E_-| = 2$:

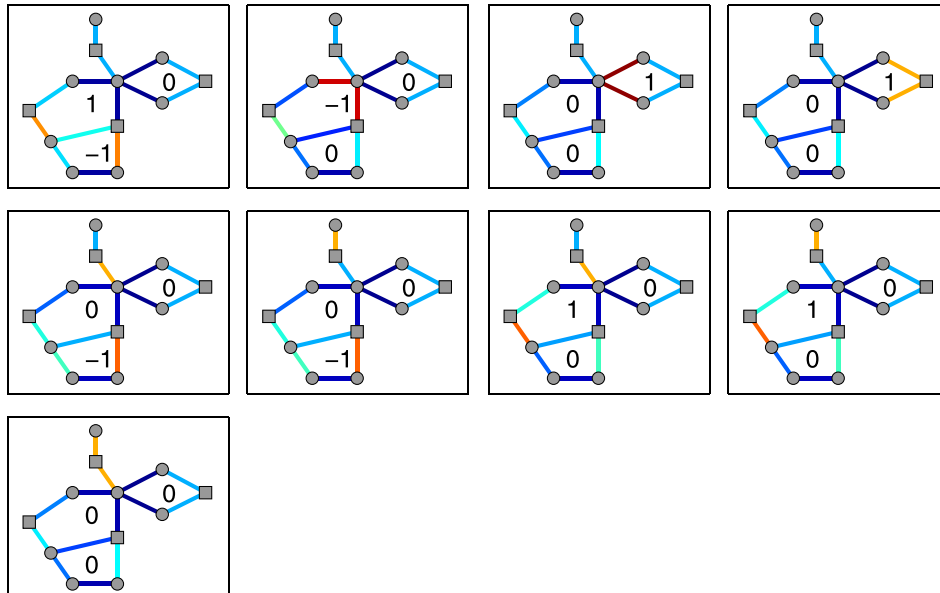


FIG. 12. All fixed points with $|E_-| \leq 2$ in a network with three cycles calculated using the algorithm described in the main text. The winding number of each cycle is displayed. Squares represent the generators with $P = +2P_0$ and circles the consumers with $P = -P_0$. All links have a coupling strength of $K = 24/19 \times P_0$.

Kuramoto's seminal work² has been devoted to the onset of partial synchronization in large networks. However, in some applications, global synchronization is required. In particular, in electrical power grids, all generators have to run with exactly the same frequency and have to be strictly phase-locked to enable stable power flows to the customers. A desynchronization generally has catastrophic consequences. An example is provided by the European power blackout in November 2006. Following a shutdown of one transmission line and unsuccessful attempts to restore stable operation, the European grid fragmented in three mutually asynchronous clusters.²³ In the end, more than 10 million customers were cut from the power supply.

In this article, we have analyzed the existence of stable fixed points in finite oscillator networks. The main methodological advancement is to split the calculation into two parts: first, we calculate the flows which satisfy the continuity equation at all nodes. Then, we single out the specific solution which leads to consistent phases of the oscillators. We thus move the focus of the calculation from the nodes (phases) to the edges (flows) and cycles. An immediate consequence is that several fixed points can co-exist, which differ by cycle flows. Thus, oscillator networks are in general multistable.

For networks containing a single cycle, we have obtained upper and lower bounds for the number of fixed points in terms of three structural quantities: the maximal partial net power \bar{P}_{\max} , which measures the homogeneity of the power injections or natural frequencies and the maximum and minimum edge strength along the cycle. We find that generally the number of stable fixed points is particularly large if (a) the cycle is long, (b) the edge strength is large, and (c) the power sources are distributed homogeneously. However, the example discussed in Sec. IV D shows that extreme care has to be taken for special network topologies. Increasing the strength of the wrong edge can also decrease the number of fixed points. Finding bounds for the number of stable fixed points in general network topologies is much more involved. The results have been obtained for planar networks, but the bounds are much weaker as for networks with single cycles. Interestingly, both tree networks and fully connected networks have at most one stable fixed point. However, networks with intermediate sparsity, which is most realistic for electrical power grids, may exhibit multistability.

Several aspects of multistability have been previously discussed in the literature. Multistability in isolated rings was discussed in Ref. 38. The limits (92) were derived, and the basins of attraction of the different fixed points were studied numerically. The case of a densely connected graph was analyzed by Taylor in Ref. 41. He was able to show that there is at most one stable fixed point if the node degree is at least $0.9395 \times (N - 1)$. Mehta *et al.* investigate multistability in complex networks numerically using a similar approach to the present paper.⁴³ They argue that the number of fixed points scales with the number of cycles as each cycle can accommodate cycle flows. While this is valid for many graphs, there are counterexamples (Fig. 7). Delabays *et al.*³⁷ have recently reported their treatment of multistability using

cycle flows. They have extended the upper bounds for fixed points in single rings in Ref. 38 to also include those stable fixed points with phase differences along edges $> \pi/2$. They have also derived upper bounds⁵¹ for a number of fixed points for planar graphs in the case of uniform power injections at all nodes. Xi *et al.*⁵⁵ have numerically shown that the spatial heterogeneity of power injections P_j reduces the number of fixed points, which fits with our analytical result in Corollary 3. Intriguingly, they have also found that in heterogeneous ring topologies, the nonlinear stability of fixed points decreases with the ring size N .

In this work, we have obtained a *lower bound* for the number of fixed points and thereby provided a *sufficient condition* for the existence of multistability. Furthermore, we have shown that the length of the cycles N_c and the homogeneity \bar{P}_{\max} are equally important for multistability and thereby arrived at tighter bounds for the number of fixed points than Ochab and Gora³⁸ and Delabays *et al.*³⁷ Moreover, we have derived scaling laws at the limit of infinite transmission strengths that are much tighter than the upper bound results previously reported. We have shown the derived scaling behaviour to match numerically computed exact results for moderately sized networks.

Interestingly, our results show that a previous highly recognized result presented by Jadbabaie *et al.* in Ref. 57 is incorrect. The authors claim that for any network of Kuramoto oscillators with different natural frequencies, there exists a K_u such that for $K > K_u$ there is only one stable fixed point. This claim is disproven by the examples presented in Sec. IV C as well as by the rigorous results on the existence of multiple fixed points in Corollary 3. The error in the proof of Ref. 57 is rather technical. The authors define a function \mathbf{L} such that the defining equation of a fixed point (4) can be rewritten in the form

$$\boldsymbol{\theta}^* = \mathbf{L}(\boldsymbol{\theta}^*). \quad (129)$$

Jadbabaie *et al.* then claim that \mathbf{L} is a contraction on the subset of $\boldsymbol{\theta}$ such that $|\theta_i - \theta_j| < \pi/2$ for all edges (i, j) , which we called normal operation. Banach's contraction theorem then yields that the algebraic equation (129) has a unique fixed point. The problem is that the range of $\mathbf{L}(\boldsymbol{\theta})$ is generally *not* a subset of subspace of normal operation, even if the domain is. After applying \mathbf{L} , some phase differences can get out of the interval $[-\pi/2, \pi/2]$. Thus, Banach's contraction theorem cannot be applied, which spoils the proof.

IX. CONCLUSION

In summary, taking cycle flows as a basis of flow patterns, we analyzed the existence and stability of phase locked states in networks of Kuramoto oscillators and second order phase oscillators modeling the phase dynamics of electric power grids. We demonstrated that such systems exhibit multistability. Intriguingly, multistability prevails even under conditions where unique stable operating points were believed to exist in both a power engineering textbook and a major complex network reference on Kuramoto oscillators.^{56,57} For classes of network topologies, we have established necessary and sufficient conditions for multistability

and derived lower and upper bounds for the number of fixed points. We explained why generalizing those bounds for arbitrary topologies is hard. Nevertheless, we have derived asymptotic scaling laws at a large loop limit that has been found to match closely numerically obtained exact results.

ACKNOWLEDGMENTS

We gratefully acknowledge support from the Federal Ministry of Education and Research (BMBF Grant No. 03SF0472A-E), the Helmholtz Association (via the joint initiative “Energy System 2050 – A Contribution of the Research Field Energy” and the Grant No. VH-NG-1025 to D.W.) and the Max Planck Society to M.T. The works of D.M. were supported by the IMPRS Physics of Biological and Complex Systems, Göttingen.

- ¹C. Huygens, *Oeuvres Complètes de Christiaan Huygens* (Martinus Nijhoff, The Hague, The Netherlands, 1893).
- ²Y. Kuramoto, in *International Symposium on Mathematical Problems in Theoretical Physics*, Lecture Notes in Physics Vol. 39, edited by H. Araki (Springer, New York, 1975), p. 420.
- ³Y. Kuramoto, *Chemical Oscillations, Waves, and Turbulence* (Springer, Berlin, 1984).
- ⁴K. Wiesenfeld, P. Colet, and S. H. Strogatz, *Phys. Rev. Lett.* **76**, 404 (1996).
- ⁵F. Varela, J.-P. Lachaux, E. Rodriguez, and J. Martinerie, *Nat. Rev. Neurosci.* **2**, 229 (2001).
- ⁶I. Z. Kiss, Y. Zhai, and J. L. Hudson, *Science* **296**, 1676 (2002).
- ⁷S. H. Strogatz, *Phys. D: Nonlinear Phenom.* **143**, 1 (2000).
- ⁸J. A. Acebrón, L. L. Bonilla, C. J. Pérez Vicente, F. Ritort, and R. Spigler, *Rev. Mod. Phys.* **77**, 137 (2005).
- ⁹A. Arenas, A. Díaz-Guilera, J. Kurths, Y. Moreno, and C. Zhou, *Phys. Rep.* **469**, 93 (2008).
- ¹⁰D. Witthaut and M. Timme, *Phys. Rev. E* **90**, 032917 (2014).
- ¹¹B. Ermentrout, *J. Math. Biol.* **29**, 571 (1991).
- ¹²S.-Y. Ha, E. Jeong, and M.-J. Kang, *Nonlinearity* **23**, 3139 (2010).
- ¹³S. H. Strogatz, D. M. Abrams, A. McRobie, B. Eckhardt, and E. Ott, *Nature* **438**, 43 (2005).
- ¹⁴A. R. Bergen and D. J. Hill, *IEEE Trans. Power Appar. Syst.* **PAS-100**, 25 (1981).
- ¹⁵G. Filatrella, A. H. Nielsen, and N. F. Pedersen, *Eur. Phys. J. B* **61**, 485 (2008).
- ¹⁶M. Rohden, A. Sorge, M. Timme, and D. Witthaut, *Phys. Rev. Lett.* **109**, 064101 (2012).
- ¹⁷A. E. Motter, S. A. Myers, M. Anghel, and T. Nishikawa, *Nat. Phys.* **9**, 191 (2013).
- ¹⁸F. Dörfler, M. Chertkov, and F. Bullo, *Proc. Natl. Acad. Sci.* **110**, 2005 (2013).
- ¹⁹M. Rohden, A. Sorge, D. Witthaut, and M. Timme, *Chaos* **24**, 013123 (2014).
- ²⁰B. Schäfer, M. Matthiae, M. Timme, and D. Witthaut, *New J. Phys.* **17**, 015002 (2015).
- ²¹M. E. J. Newman, *Networks—An Introduction* (Oxford University Press, Oxford, 2010).
- ²²D. Witthaut, M. Rohden, X. Zhang, S. Hallerberg, and M. Timme, *Phys. Rev. Lett.* **116**, 138701 (2016).
- ²³Union for the Coordination of Transmission of Electricity, https://www.entsoe.eu/fileadmin/user_upload/_library/publications/ce/otherreports/Final-Report-20070130.pdf for Final report on the system disturbance; accessed 4 November 2006 (2007).
- ²⁴S. Watanabe and S. H. Strogatz, *Phys. Rev. Lett.* **70**, 2391 (1993).
- ²⁵C. Bick, M. Timme, D. Paulikat, D. Rathlev, and P. Ashwin, *Phys. Rev. Lett.* **107**, 244101 (2011).
- ²⁶G. Filatrella, N. F. Pedersen, and K. Wiesenfeld, *Phys. Rev. E* **61**, 2513 (2000).
- ²⁷G. Filatrella, N. F. Pedersen, and K. Wiesenfeld, *Phys. Rev. E* **75**, 017201 (2007).
- ²⁸S. Gupta, A. Campa, and S. Ruffo, *J. Stat. Mech.: Theory Exp.* **2014**, R08001.
- ²⁹D. Manik, D. Witthaut, B. Schäfer, M. Matthiae, A. Sorge, M. Rohden, E. Katifori, and M. Timme, *Eur. Phys. J. Spec. Top.* **223**, 2527 (2014).
- ³⁰T. Coletta and P. Jacquod, *Phys. Rev. E* **93**, 032222 (2016).
- ³¹L. G. Khazin and E. Schnol, *Stability of Critical Equilibrium States* (Manchester University Press, 1991).
- ³²C. J. Tavora and O. J. Smith, *IEEE Trans. Power Appar. Syst.* **PAS-91**, 1138–1144 (1972).
- ³³E. Katifori, G. J. Szöllösi, and M. O. Magnasco, *Phys. Rev. Lett.* **104**, 048704 (2010).
- ³⁴H. Ronellenfitsch, M. Timme, and D. Witthaut, *IEEE Trans. Power Syst.* **32**, 1007 (2016).
- ³⁵R. Diestel, *Graph Theory* (Springer, New York, 2010).
- ³⁶C. Godsil and G. F. Royle, *Algebraic Graph Theory* (Springer Science & Business Media, 2013), Vol. 207.
- ³⁷R. Delabays, T. Coletta, and P. Jacquod, *J. Math. Phys.* **57**, 032701 (2016).
- ³⁸J. Ochab and P. Gora, *Acta Phys. Pol. Ser. B, Proc. Suppl.* **3**, 453 (2010).
- ³⁹D. A. Wiley, S. H. Strogatz, and M. Girvan, *Chaos: Interdiscip. J. Nonlinear Sci.* **16**, 015103 (2006).
- ⁴⁰M. Wolf, F. Verstraete, and J. Cirac, *Int. J. Quantum Inf.* **1**, 465 (2003).
- ⁴¹R. Taylor, *J. Phys. A: Math. Theor.* **45**, 055102 (2012).
- ⁴²F. Ionita, D. Labavic, M. A. Zaks, and H. Meyer-Ortmanns, *Eur. Phys. J. B* **86**, 511 (2013).
- ⁴³D. Mehta, N. Daleo, F. Dörfler, and J. D. Hauenstein, *Chaos* **25**, 053103 (2015).
- ⁴⁴A. Korsak, *IEEE Trans. Power App. Syst.* **PAS-91**, 1093 (1972).
- ⁴⁵D. Witthaut and M. Timme, *New J. Phys.* **14**, 083036 (2012).
- ⁴⁶D. Witthaut and M. Timme, *Eur. Phys. J. B* **86**, 377 (2013).
- ⁴⁷D. Braess, *Unternehmensforschung* **12**, 258 (1968).
- ⁴⁸Y. Nussbaum, preprint [arXiv:1012.4767](https://arxiv.org/abs/1012.4767) (2010).
- ⁴⁹L. R. Ford, Jr. and D. R. Fulkerson, *Flows in Networks* (Princeton University Press, 2015).
- ⁵⁰S. Mac Lane, *Fundam. Math.* **28**, 22 (1937).
- ⁵¹R. Delabays, T. Coletta, and P. Jacquod, *J. Math. Phys.* **58**, 032703 (2017).
- ⁵²P. J. Menck, J. Heitzig, N. Marwan, and J. Kurths, *Nat. Phys.* **9**, 89 (2013).
- ⁵³H.-D. Chiang, F. Wu, and P. Varaiya, *IEEE Trans. Circuits Syst.* **34**, 160 (1987).
- ⁵⁴B. Schäfer, M. Matthiae, X. Zhang, M. Rohden, M. Timme, and D. Witthaut, *Phys. Rev. E* **95**, 060203 (2017).
- ⁵⁵K. Xi, J. L. Dubbeldam, and H. X. Lin, *Chaos: Interdiscip. J. Nonlinear Sci.* **27**, 013109 (2017).
- ⁵⁶A. Jadbabaie, N. Motee, and M. Barahona, in *Proceedings of the 2004 American Control Conference* (IEEE, 2004), Vol. 5, pp. 4296–4301.
- ⁵⁷J. Machowski, J. Bialek, and J. Bumby, *Power System Dynamics, Stability and Control* (John Wiley & Sons, New York, 2008).
- ⁵⁸W. Chen, D. Wang, J. Liu, T. Basar, K. H. Johansson, and L. Qiu, *IFAC-PapersOnLine* **49**(22), 97–102 (2016).